creative commons
COMMONS DEED

저작자표시-비영리-변경금지 2.0 대한민국

이용자는 아래의 조건을 따르는 경우에 한하여 자유롭게

- 이 저작물을 복제, 배포, 전송, 전시, 공연 및 방송할 수 있습니다.

다음과 같은 조건을 따라야 합니다:

저작자표시. 귀하는 원저작자를 표시하여야 합니다.

비영리. 귀하는 이 저작물을 영리 목적으로 이용할 수 없습니다.

변경금지. 귀하는 이 저작물을 개작, 변형 또는 가공할 수 없습니다.

- 귀하는, 이 저작물의 재이용이나 배포의 경우, 이 저작물에 적용된 이용허락조건을 명확하게 나타내어야 합니다.
- 저작권자로부터 별도의 허가를 받으면 이러한 조건들은 적용되지 않습니다.

저작권법에 따른 이용자의 권리는 위의 내용에 의하여 영향을 받지 않습니다.

이것은 이용허락규약(Legal Code)을 이해하기 쉽게 요약한 것입니다.

Disclaimer

dCollection

치의과학박사 학위논문

Fit analysis of the stereolithography-manufacturing three-unit resin prosthesis with various 3D-printing build orientations and layer thicknesses

Stereolithography 방식으로 제작된 3 본 레진 보철물의 다양한 3D 프린팅 적층 방향과 두께에 따른 적합도 분석

2021 년 2 월

서울대학교 대학원

치의과학과 치과보철학 전공

장 계 준

Fit analysis of stereolithography-manufacturing three-unit resin prosthesis with various 3D-printing build orientations and layer thicknesses

지도교수 김 성 균

이 논문을 장계준 박사학위논문으로 제출함

2020 년 12 월

서울대학교 대학원

치의과학과 치과보철학 전공

장 계 준

장계준의 박사학위논문을 인준함

2021 년 1 월

위 원 장 허 성 주 (인)

부 위 원 장 김 성 균 (인)

위 원 곽 재 영 (인)

위 원 양 형 철 (인)

위 원 김 형 섭 (인)

-ABSTRACT-

Fit analysis of stereolithography-manufacturing three-unit resin prosthesis with various 3D-printing build orientations and layer thicknesses

Gaejun Jang, D.D.S., M.S.D

Department of Prosthodontics, Graduate School, Seoul National University

(Directed by Professor Seong-Kyun Kim, D.D.S., M.S.D., Ph.D.)

Purpose: The purpose of this study was to analyze the fit according to the build orientations and layer thicknesses in stereolithography (SLA) manufactured three-unit resin prostheses.

Materials and methods: A master model was fabricated with 5-axis milling machine (IDC MILL 5X; Amann girrbach AG, Koblach, Austria) for the three-unit resin fixed partial denture. After scanning (T500; Medit, Seoul, Korea) the master model, prosthesis design was proceeded using CAD software (Exocad Dental CAD; Exocad GmbH, Darmstadt, Germany), and then 3D printed prostheses were produced using a stereolithography (SLA) 3D printer (Zenith U; Dentis, Daegu, Korea). The angle formed between the long axis of the abutment and build direction was defined as the build

orientation. The prostheses were produced in five build orientations (0°, 30°, 45°, 60° and 90°) and two-layer thicknesses (50 μm and 100 μm) (n=10 for each group). For milled group, ten specimens were produced with the same CAD design using a 5-axis milling machine (Arum DEG-5X100; Doowon, Seoul, Korea). The prostheses were mounted on the master model, and CT scan was done using a micro-CT scanner (Skyscan 1172; Bruker micro-CT, Kontich, Belgium).

For quantitative analysis, marginal and internal fits were measured using imageJ software (ImageJ 1.52 version; NIH, Bethesda, MD, USA). Marginal fits were measured as the absolute marginal discrepancy (AMD) and marginal gap (MG). Internal fits were measured as the cervical area (CE), mid axial wall area (AX), line-angle area (LA) and occlusal area (OC). AX was divided into inner/outer/buccal/lingual AX for more precise evaluation. Internal gap volume (IGV) was measured using CTAn software (CTAn 1.17.7.2 version; Bruker micro-CT, Kontich, Belgium). For statistical analysis, two-way ANOVA and independent T-test were used. The confidence level was set to a value of 95% for all statistical analysis.

For qualitative analysis, coronal, sagittal and horizontal CT cross sections were examined and characteristic differences among the groups were compared. Internal surface of each specimen was imaged with SEM (Apreo S LoVac; Thermo Fisher Scientific, Brno, Czech) and microstructural characteristics were analyzed.

Results: The smallest AMD was 71.9 ± 8.3 μm (50 μm, 45°) and the largest value was 121.6 ± 12.5 μm (50 μm, 90°). The smallest MG was 41.6 ± 7.2 μm (50 μm, 45°) and

the largest value was 84.4 ± 12.3 μm (50 μm, 90°). The build orientation 30° and 45° groups presented preferable marginal fits than other build orientations for both layer thicknesses. The smallest CE was 67.1 ± 8.4 μm (50 μm, 60°) and the largest value was 122.1 ± 9.2 μm (50 μm, 0°). The smallest AX was 79.0 ± 8.2 μm (50 μm, 60°) and the largest value was 115.0 ± 11.3 μm (50 μm, 0°). The build orientation 60° groups presented smaller CE and AX values than other build orientations for both layer thicknesses. Furthermore, inner AX (141.9 ± 23.7 μm for 50 μm, 172.3 ± 23.2 μm for 100 μm) was larger than the outer AX (92.7 ± 17.8 μm for 50 μm, 74.0 ± 16.6 μm for 100 μm) for printed groups ($p < 0.001$). Sagittal AX values decreased with build orientation increase from 0° to 60° but increased in 90° build orientation. The smallest LA was 65.7 ± 6.5 μm (100 μm, 90°) and the largest value was 102.3 ± 8.0 μm (100 μm, 30°). The smallest OC was 97.4 ± 25.5 μm (50 μm, 30°) and the largest value was 206.0 ± 16.7 μm (100 μm, 0°). The smallest IGV was 20.2 ± 1.2 mm^3 (50 μm, 60°) and the largest volume was 25.5 ± 1.3 mm^3 (100 μm, 30°). IGV was smallest with 60° build orientation regardless of the layer thickness. Except for the 0° build orientation, 50 μm groups showed smaller IGV values than the 100 μm groups for each build orientation.

The AMD and CE of 3D printed groups with desirable conditions (50 μm, 45° and 60°) were significantly smaller than those of milled group. However, the MG and LA of 3D printed groups were significantly larger than those of milled group.

A stair-shaped appearance was observed for all printed groups. This shape appeared more prominently in 100 μm groups than 50 μm groups. Surface smoothness was better for milled specimens compared to printed specimens. From the horizontal CT section, the inner AX was larger than the outer AX in the printed groups. In sagittal CT section,

irregular inner occlusal surface was observed in 0° groups and large wavy, uneven surface patterns on the inner buccal surface was observed in 90° groups. From the SEM photographs, voids on the inner occlusal surface were observed in 0° groups and large voids on the inner buccal surface were observed in 90° groups. Additionally, 90° specimens presented the vertical lines and flaws parallel to the build direction on the inner occlusal surface. The size of the void was larger in 100 μm layer thickness groups compared to the 50 μm groups.

Conclusions: For SLA 3D printed resin prostheses, a difference in fit occurred based on the printing conditions. The desired printing conditions considering the marginal and internal fit were a 50 μm layer thickness with 45° and 60° build orientations. The same conclusion can be drawn with the SEM analysis because unintentional voids were created on the inner surface for 0° and 90° groups. When the SLA 3D printed prosthesis is manufactured with proper conditions, it is possible to obtain a comparable fit to the milled prosthesis. The fitness of both 3D printed and milled prostheses showed a clinically acceptable fit.

Keywords : Stereolithography; 3D printing; Micro-CT; Fit; Build orientation; Layer thickness

Student Number : 2018-30853

CONTENTS

I. INTRODUCTION

In the most recent century, computer-aided design/computer-aided manufacturing (CAD/CAM) technology has been rapidly developed and has changed the paradigm of dental treatment.[1] Variety types of dental prostheses have been manufactured through the CAD/CAM method in the dental field for decades.[2] This change made a paradigm shift of dental implant treatment and influenced on the dental implant prostheses manufacturing.[3] CAD/CAM method enables the immediate restoration on the day of surgery using pre-fabricated prosthesis, right after the dental implant installation with an accurate surgical guide.[4,5] In contrary, lost wax technique was used to produce conventional prosthesis in the past time which had a time-consuming drawback. In addition, many errors were made by lab technician due to the manufacturing process limitations.[6,7]

The CAM method is classified into additive and subtractive manufacturing. Three-dimensional (3D) printing is a layer-by-layer additive manufacturing method. Milling is a subtractive manufacturing method to cut down the blocks to fabricate the desired shapes of the prostheses. Although both methods have pros and cons, additive manufacturing has the advantage that noise, heat and waste generation is reduced and milling burs do not need to be replaced.[8-10]

Additive manufacturing is classified into 7 categories according to the American Society of Testing and Materials (ISO/ASTM 52900): binder jetting, directed energy deposition, material extrusion, material jetting, powder bed fusion, sheet lamination and vat polymerization.[11] Utilizing this classification, the 3D-printing methods that are most

frequently used can be easily categorized: stereolithography (SLA, vat polymerization), digital light processing (DLP, vat polymerization), fused deposition modelling (FDM, material extrusion), selective laser sintering (SLS, powder bed fusion) and laminated object manufacturing (LOM, sheet lamination).[11,12] FDM method is also called fused filament fabrication (FFF). This method produces the result by injecting after liquefying the filament materials. SLS method is also called selective laser melting (SLM) when manufacturing metal result. The scanning laser is irradiated on the powder bed, fusion occurs at just below the melting point while the platform descends during manufacturing to produce the result. LOM method uses plastic or paper sheets and heated roller enables lamination between the sheets. SLA and DLP methods have been widely used among these 3D printing methods. The DLP method uses UV light to photopolymerize the cross section in the x-y plane. The part corresponding to the cross section is irradiated, and the platform moves to the z-axis direction during manufacturing. The SLA method is similar to DLP. However, when printing the x-y plane, the major difference is that the SLA uses a single laser point during manufacturing.[13,14] The drawback of SLA to the DLP type is that the build time increases.[13,15] However, the SLA-manufactured prostheses provide a much more precise configuration and smoother surface finish compared to other printing methods such as SLS, FDM and LOM.[12,16]

SLA additive manufacturing has been widely used from the past.[17,18] With the development of SLA additive manufacturing, even wax pattern and zirconia materials can be handled in presence.[19-21] In a previous study, metal copings produced by the SLA method was superior compared to the milling method.[20,21]

Provisional implant prostheses can be fabricated easily using a 3D printer with a

certain reproducibility. In the past, provisional restorations were made intra-orally by direct method. Moulding and Teplitsky[22] proposed that the direct method may cause pulp damage due to the released polymerizing heat. Indirect method can avoid this disadvantage and has certain advantage to reproduce the anatomical tooth form in provisional restorations.[23] According to Burns' review article[24], abutment protection and improving aesthetic requirements are recommended for provisional prostheses. Marginal and internal adaptations are prerequisites for successful dental restorations.[25-27] An ill-fitting prosthesis may cause cement washout, loss of retention, plaque accumulation and compromised periodontal health.[28-30] Furthermore, the accuracy of the immediate implant provisional restoration is extremely important because it can reduce the chair time and improve patient satisfaction.[31,32]

In a previous study, a 135° (45° in this paper) build angle presented excellent accuracy with the DLP method.[33] Park et al.[34] evaluated the fit of DLP 3D printed prostheses with different conditions and concluded that 45° and 60° build orientations were preferable. There was a marginal gap difference according to layer thickness, but the effect was not significant. On the other hand, some studies have shown marginal discrepancies at a fixed build orientation.[35,36]

With SLA technology, superior precision was achieved for milling rather than printing for a single crown case.[37] However, only a fixed build orientation was applied without considering the optimal printing conditions.

The fit difference could be related to the microstructural change of the prosthesis due to the printing conditions. A sagging effect could occur due to the gravity and the

physical properties of the materials.[38] Even a simply shaped prosthesis may have dimensional changes.[39] Alharbi et al.[40] reported that the self-supported surface may change depending on the build direction. Therefore, it can be assumed that the printing conditions may affect the prosthesis structure.

Summarizing the previous studies on SLA 3D printing techniques, there has been no research published to date with anatomical teeth shaped three-unit fixed partial dentures (FPDs) that analyzes the effects of build orientation and layer thickness simultaneously. Investigation of the microstructural differences using micro computed tomography (micro-CT) and scanning electron microscopy (SEM) can provide a more visible and intuitive understanding of the effects of printing conditions. To date, no studies have investigated in detail using these methods.

The purpose of this study was to analyze the fit according to the build orientations and layer thicknesses in SLA manufactured three-unit resin prostheses. The null hypotheses were: (a) that there is no difference in fit among all 3D printed groups and (b) that there is no difference in fit between the milled and 3D printed groups.

II. MATERIALS AND METHODS

A. Model and prostheses fabrication

A-1. Master model design and fabrication

A master model was designed for a three-unit resin fixed partial denture with two implant abutments (Fig. 1). Three-dimensional configurations of the abutments were set considering the real anatomical size of the mandibular second premolar and second molar assuming the #45 and #47 teeth.[41] Since a 10° to 20° convergence angle is recommended in previous study[42], the total convergence angle of the abutments was set to 14.3°. One millimeter of shoulder margin was given to each abutment. Cone-shaped reference points with 1mm in both diameter and height were designed below the margin of each abutment. Reference points were used to determine the coronal and sagittal reference planes to obtain sectional view of the specimens.

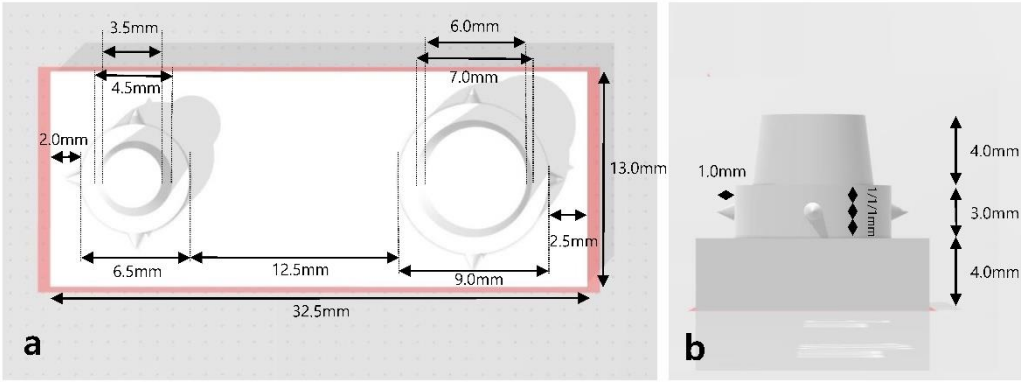

Figure 1. CAD design of the model. (a) occlusal view and (b) distal view.

Standard triangulated language (STL) file of the master model was obtained using the CAD software (Rhinoceros 5.0; McNeel, Seattle, USA). A polymethylmethacrylate (PMMA) resin block (Yamahachi dental MFG, Ochigara, Japan) was milled with a 5-axis milling machine (IDC MILL 5X; Amann girrbach AG, Koblach, Austria) using the STL file (Fig. 2).

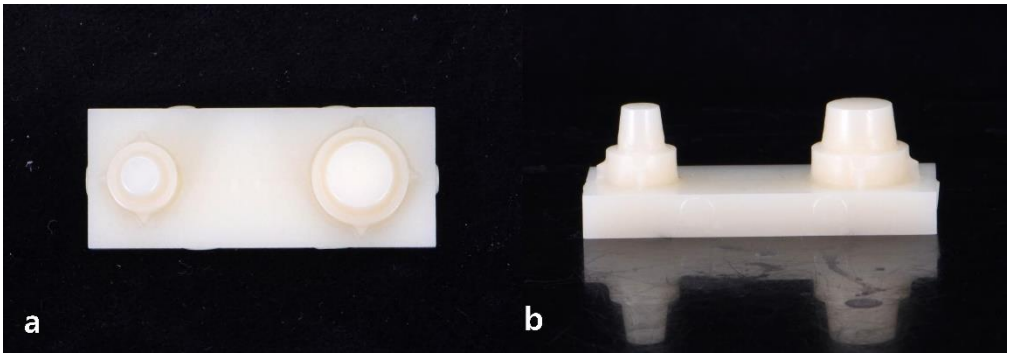

Figure 2. PMMA resin model. (a) occlusal view and (b) lingual view.

A-2. Prosthesis design and fabrication

The master model was scanned with a laboratory scanner (T500; Medit, Seoul, Korea). Anti-reflective powder (IP scan spray; IP-division, Haimhausen, Germany) was sprayed before scanning. Scanned model data were exported in STL file. The 3-unit FPD was designed on that model scan data using CAD software (Exocad Dental CAD; Exocad GmbH, Darmstadt, Germany) (Fig. 3). Cement space was set to 100 μm based on the pilot study[43], which was the was the minimum cement space value required to seat the prostheses without interference. Cement space was evenly applied to the whole surfaces of the abutments. Horizontal margin border was set to 0.1mm which was minimal value. Other margin design parameters were set to 0 value such as angled

margin border, vertical margin border, angle of margin border and below margin border. The prostheses were designed considering the real anatomical teeth morphology.[41]

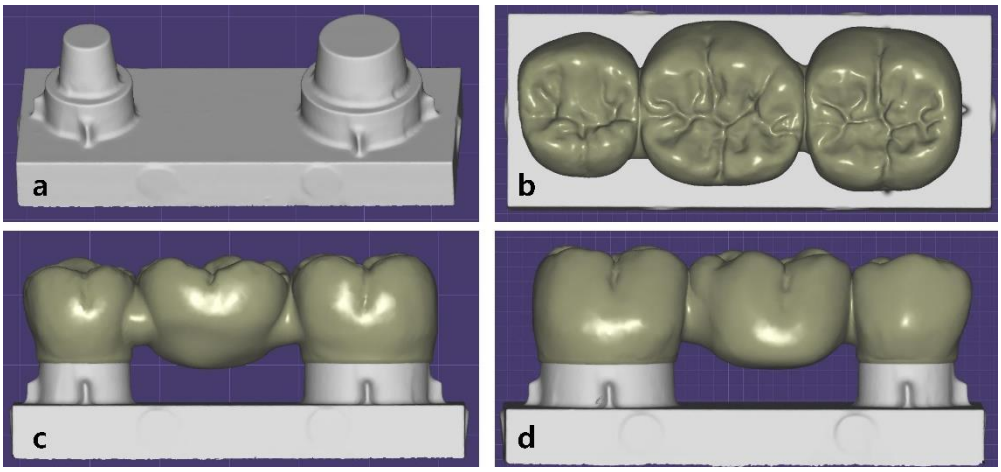

Figure 3. CAD design of the prosthesis. (a) scanned master model, (b) occlusal view, (c) lingual view and (d) buccal view.

A-2-1. 3D printing prosthesis

A hundred specimens were produced using a SLA 3D printer (Zenith U; Dentis, Daegu, Korea) (Fig. 4). The specifications of 3D printer are presented in Table 1. Temporary resin (Zenith ZMD-1000B; Dentis, Daegu, Korea) was used for the 3D printing resin material. The specifications of material as reported by manufacturer are presented in Table 2. The angle formed between the long axis of the abutment and build direction was defined as the build orientation. A thickness of single build layer along the build direction was defined as the layer thickness. The prostheses were produced in five build orientations (0°, 30°, 45°, 60° and 90°) and two-layer thicknesses (50 μm and

100 μm) (n=10 for each group) (Fig. 5).

Figure 4. SLA 3D printer used in this study (Zenith U; Dentis, Daegu, Korea).

Table 1. The specifications of 3D printer.

Build volume	110 x 110 x 150 (X,Y,Z / mm)
Layer thickness	16 μm, 50 μm, 100 μm
Dimension/ Weight	354 x 366 x 483 mm / 17.5kg
Light source	Blue Laser
Power	120 W

Table 2. The specifications of 3D printing resin material.

Flexural strength (MPa)	80
Water absorption (μg/mm^3)	< 40
Water solubility (μg/mm^3)	< 5

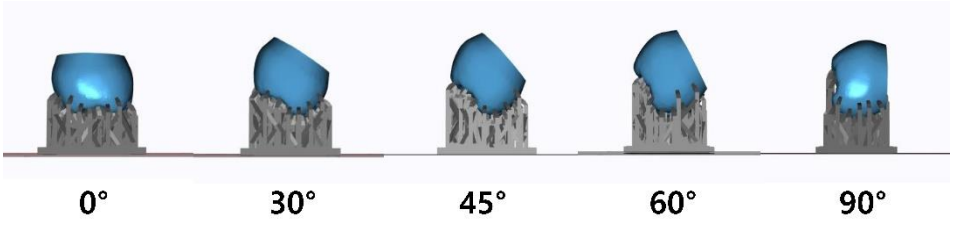

Figure 5. Distal view of the prostheses with various build orientations (0°, 30°, 45°, 60° and 90°).

According to Unkovskiy's research[44], distortion of prosthesis can vary depending on the distance from the center of the SLA printer. Therefore, the total number of prostheses produced at once was limited to four and designed to have the same distance from the center of the platform (Fig. 6). Supporter design was applied with same condition for all specimens. Density of supporter was set to 1.8 unit/mm^2. Thickness of each supporter was 0.4 mm. Supporters were automatically attached using printer software (Zenith S/W; Dentis, Daegu, Korea).

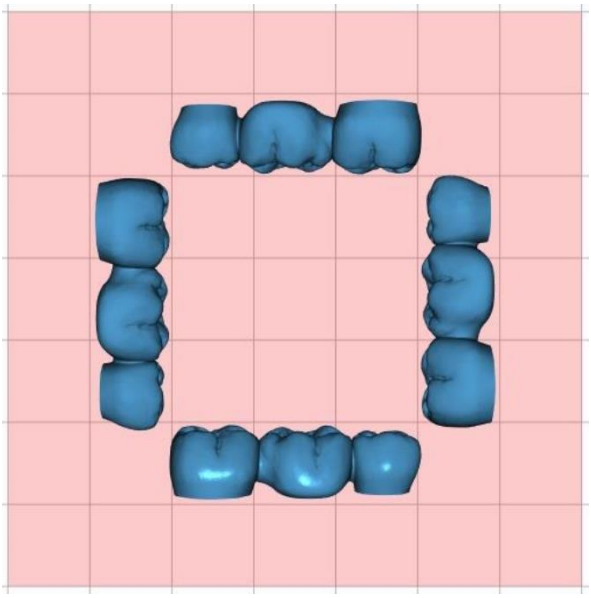

Figure 6. Four prostheses (90° build orientation) were fabricated in one plate at a time. Same distance from the center was confirmed.

Air spray and brushing was used to remove unreacted resin material after 3D printing. Prostheses were cleaned in an ultrasonic cleaner (SH-2100; Saehan ultrasonic, Seoul, Korea) with 99.8% ethanol (absolute ethanol, Koryo Chemical Eng., Seoul, Korea) for 5 minutes. Post-curing 5 minutes was done using an ultraviolet curing unit (LC-3D Print Box; Nextdent, Soesterberg, Netherlands) following the manufacturer's instructions. After post curing process, supporters were carefully removed using disks and denture burs. All prostheses were able to seat on the master model without interference (Fig. 7).

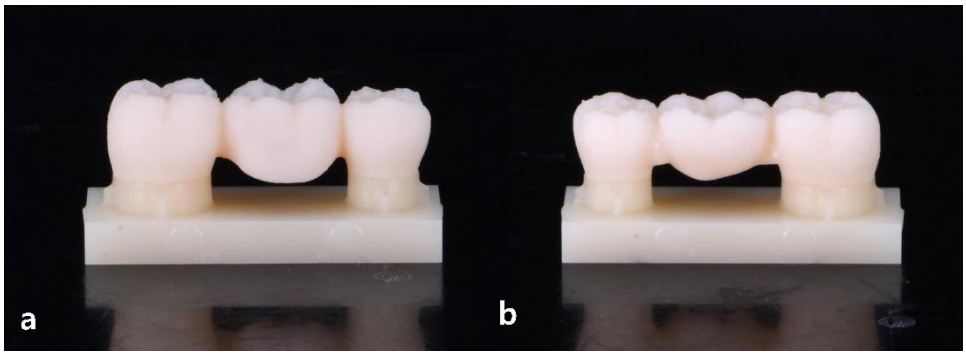

Figure 7. View of the prosthesis mounted on the master model: (a) buccal view and (b) lingual view.

A-2-2. Milling prosthesis

Ten specimens were produced with the same CAD design using a 5-axis milling machine following the manufacturer's instructions (Arum DEG-5X100; Doowon, Seoul, Korea) (Fig. 8). PMMA resin blocks (Huge PMMA block; Huge dental material, Shandong, China) were milled with 1.0, 1.5, 2.0, 3.0 mm diameter burs. The specifications of material as reported by manufacturer are presented in Table 3. Specimens were examined under magnification loupe (x4.0) for any defects, and no adjustments were made to the inner surface. All prostheses were kept in a dry, lightproof box and CT scanned within 5 days after manufacturing (Fig. 9).

Table 3. The specifications of PMMA resin block.

Flexural strength (MPa)	> 50
Water absorption (μg/mm^3)	< 40
Water solubility (μg/mm^3)	< 7.5

Figure 8. Milling machine used in this study (Arum DEG-5X100; Doowon, Seoul, Korea).

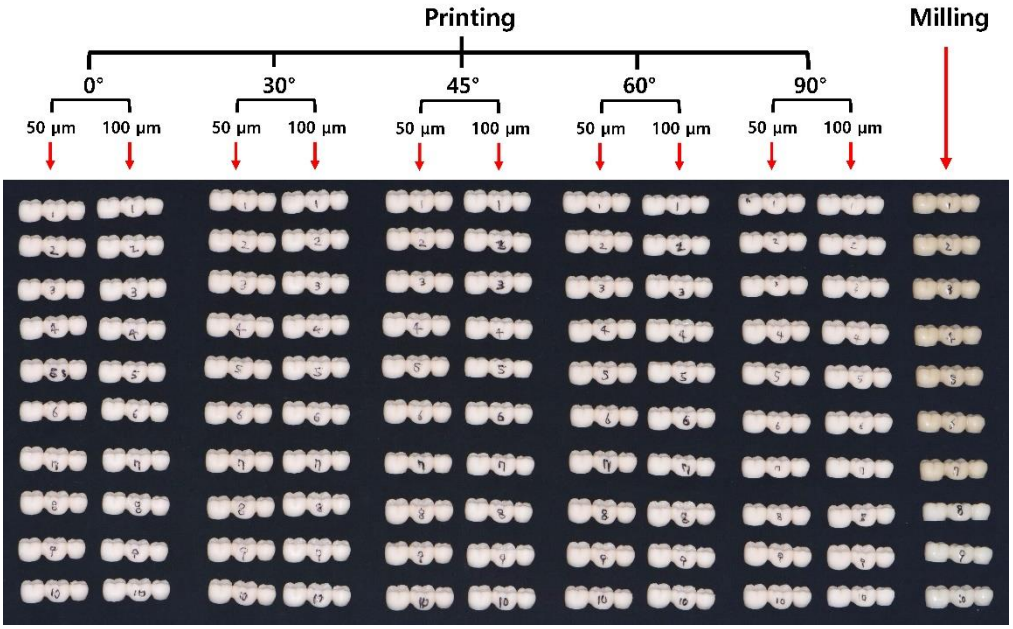

Figure 9. Total one hundred 3D printed prostheses and ten milled prostheses were fabricated.

B. Quantitative analysis

B-1. Micro-CT scan and 3D reconstruction

The model and prostheses were mounted to the jig with laboratory film (Parafilm; Bemis, Neenah, WI, USA) without cementation. CT scan was done using a micro-CT scanner (Skyscan 1172; Bruker micro-CT, Kontich, Belgium). Scanning was performed at 60 kVp and 167 μA, with an exposure time of 1475 ms. These parameters were determined based on the previous study.[34] A 0.5 mm thick aluminum filter was used and the resolution of scan was 15.44 μm. The specimen was rotated 180° with 0.7° rotational step and three frames averaging.

CT data were 3D reconstructed using NRecon software (NRecon 1.7.4.2 version; Bruker micro-CT, Kontich, Belgium). Smoothening was set to 3, ring artifact reduction was set to 8, the threshold for defect pixel mask was set to 3%, and beam-hardening correction of 20% was applied.

B-2. Marginal fit and internal fit analysis

Marginal and internal fits were measured using the imageJ software (ImageJ 1.52 version; NIH, Bethesda, MD, USA). All measurements were taken under magnification of x123. The CT cross section was obtained 20.5 times larger than the actual size, which was magnified 6 times and measured.

Marginal fits were measured as absolute marginal discrepancy (AMD) and marginal gap (MG) according to the suggestion of Holmes et al.[45] Internal fits were measured at the following sites (Fig. 10): cervical area (CE), mid axial wall area (AX), line-angle area (LA), and occlusal area (OC). The definition and division of measurement points are presented in Table 4. AX was divided into four divisions in this study for more precise evaluation: inner AX (points h and o), outer AX (points d and s), buccal AX (points 8 and 19), and lingual AX (points 4 and 15).

Cone-shaped reference points were used to determine the coronal and sagittal reference planes. The plane containing A and B reference points perpendicular to the master model base was defined as the coronal section (Fig. 11). In the coronal section, 22 points from a to v were measured. The plane containing C and D reference points perpendicular to the master model base was defined as the premolar sagittal section (Fig. 12). In the premolar sagittal section, 11 points from 1 to 11 were measured. The plane containing E and F reference points perpendicular to the master model base was defined as the molar sagittal section (Fig. 12). In the molar sagittal section, 11 points from 12 to 22 were measured.

Each measurement was repeated three times, and the mean value was used. Gap distances between prosthesis and abutment were measured at total 8 points per one specimen for AMD, MG, CE, AX and LA. Gap distances between prosthesis and abutment were measured at total 2 points per one specimen for OC.

Table 4. The definition and division of measurement points.

Division			Definition	Points
Marginal fit		AMD	The measurement from the model margin to the prosthesis margin. Absolute value was used in this study regardless of over- or under-extension. Represents 'horizontal and vertical discrepancy'.	a, k, l, v, 1, 11, 12, 22
		MG	The perpendicular measurement from the internal surface of the prosthesis to the model margin. Represents 'vertical discrepancy'.	b, j, m, u, 2, 10, 13, 21
Internal fit	Axial gap	CE	The perpendicular measurement from the abutment surface to the prosthesis at a height of 800 μm from the margin toward the occlusal plane.	c, i, n, t, 3, 9, 14, 20
		AX	The perpendicular measurement from the abutment surface to the prosthesis at a bisecting point of the axial wall.	d, h, o, s, 4, 8, 15, 19
	Occlusal gap	LA	The measurement from the line angle point of the abutment to the internal line angle point of the prosthesis.	e, g, p, r, 5, 7, 16, 18
		OC	The perpendicular measurement from the abutment surface to the prosthesis at a bisecting point of the occlusal wall.	f (same as point '6'), q (same as point '17')

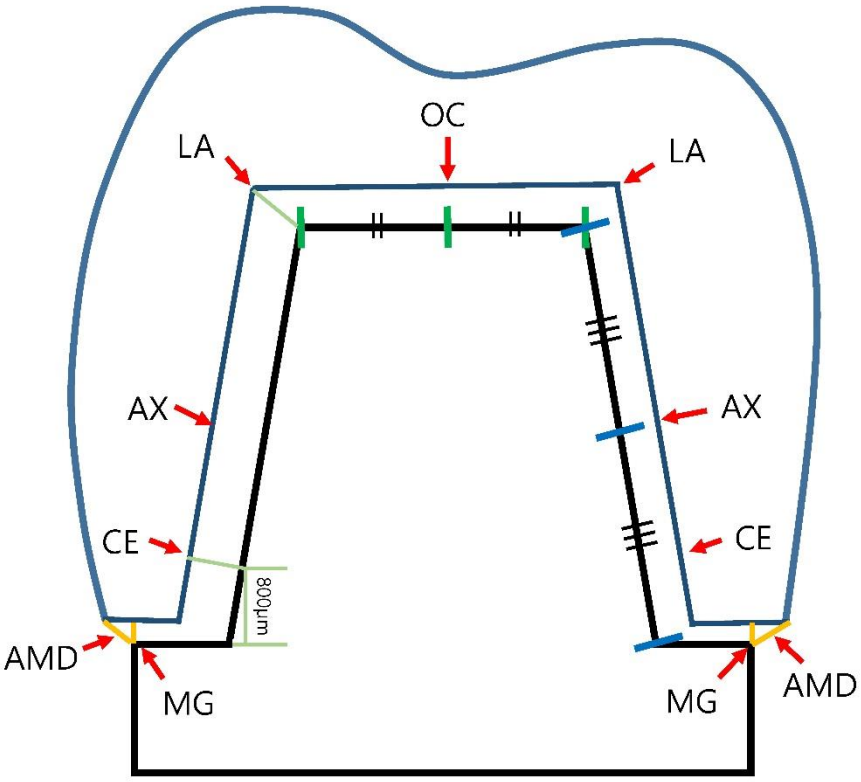

Figure 10. Measurement points of the marginal fit (AMD, MG) and internal fit (CE, AX, LA, OC). AMD: absolute marginal discrepancy, defined as the measurement from the model margin to the prosthesis margin. MG: marginal gap, defined as the perpendicular measurement from the internal surface of the prosthesis to the model margin. CE: cervical area, defined as the perpendicular measurement from the abutment surface to the prosthesis at a height of 800 μm from the margin toward the occlusal plane. AX: mid axial wall area, defined as the perpendicular measurement from the abutment surface to the prosthesis at a bisecting point of the axial wall. LA: line-angle area, defined as the measurement from the line angle point of the abutment to the internal line angle point of the prosthesis. OC: occlusal area, defined as the perpendicular measurement from the abutment surface to the prosthesis at a bisecting point of the occlusal wall.

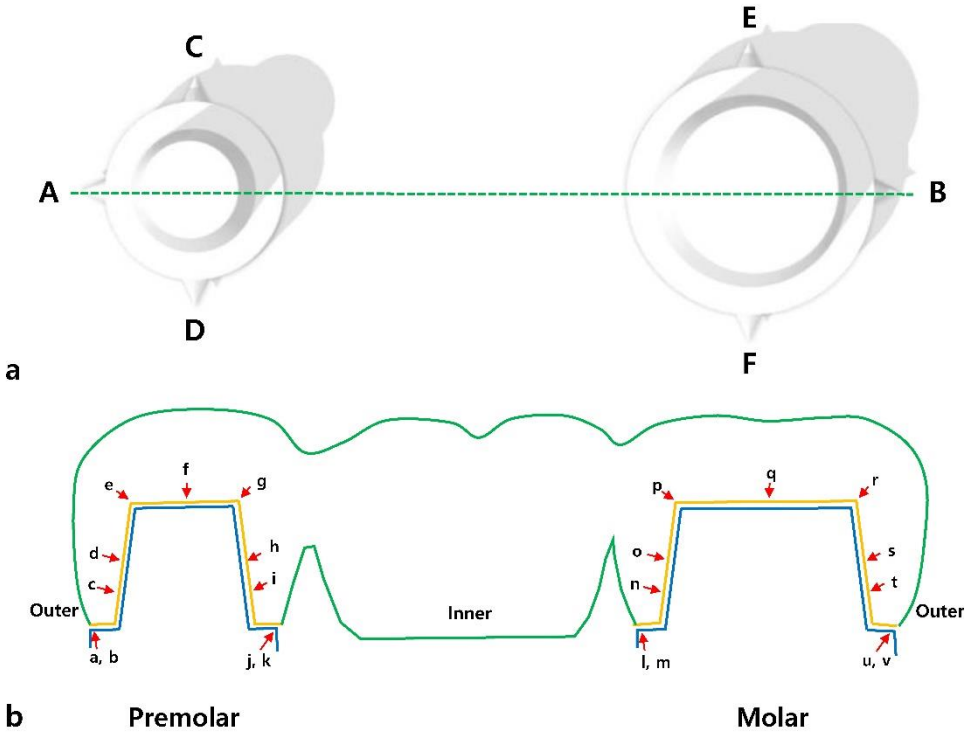

Figure 11. (a) The dotted green line represents the coronal section. (b) 22 measurement points are shown in the coronal section. AMD = points a, k, l and v. MG = points b, j, m and u. CE = points c, i, n and t. AX = points d, h, o and s. Inner AX = points h and o. Outer AX = points d and s. LA = points e, g, p and r. OC = points f and q.

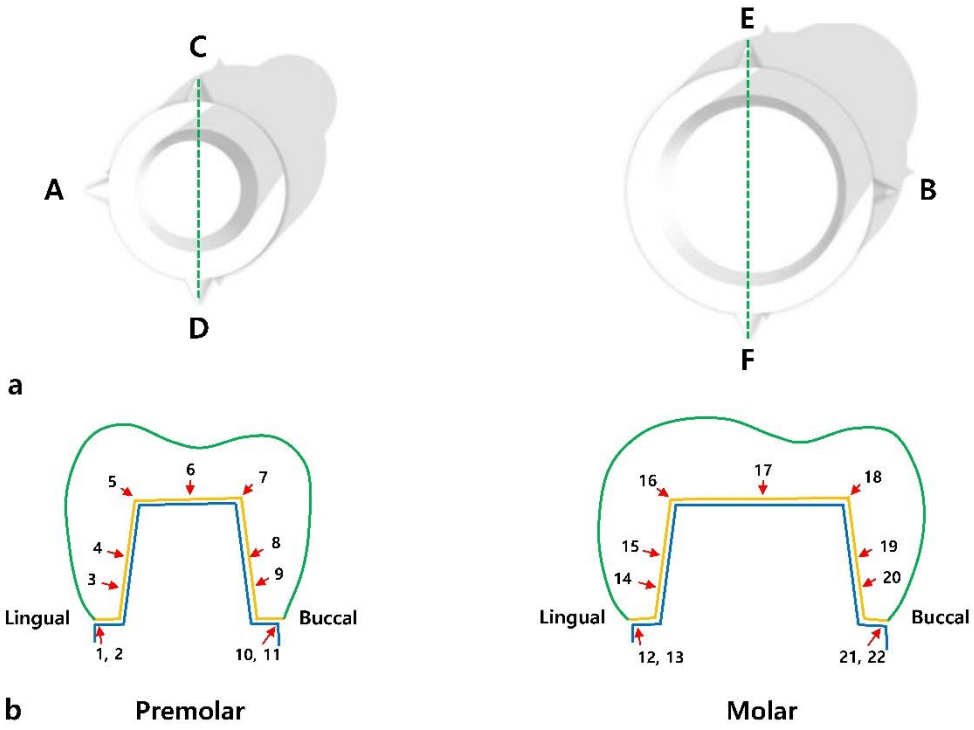

Figure 12. (a) The dotted green line represents the sagittal section. (b) 11 measurement points for each premolar and molar area are shown in the sagittal section. AMD = points 1, 11, 12 and 22. MG = points 2, 10, 13 and 21. CE = points 3, 9, 14 and 20. AX = points 4, 8, 15 and 19. Buccal AX = points 8 and 19. Lingual AX = points 4 and 15. LA = points 5, 7, 16 and 18. OC = points 6 and 17.

B-3. Internal gap volume analysis

A region of interest was set to obtain the volume between the model and the inner surface of the prosthesis. Threshold value was set from 0 to 30. Internal gap volume (IGV) was measured using CTAn software (CTAn 1.17.7.2 version, Bruker micro-CT, Kontich, Belgium). 3D reconstructed image of the IGV is shown in Figure 13.

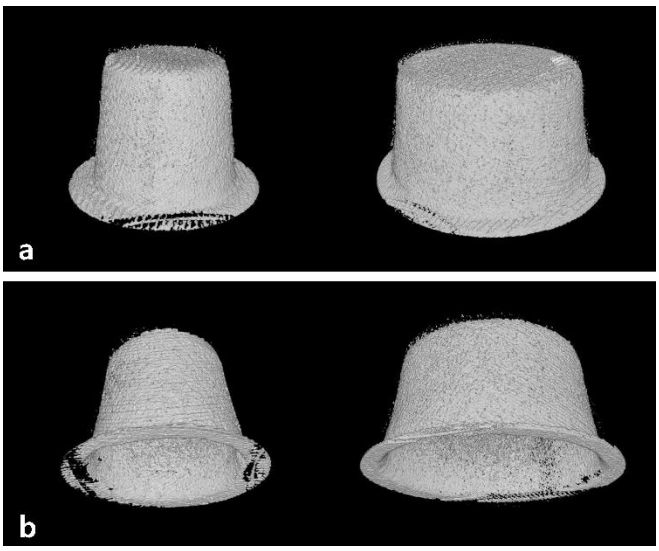

Figure 13. 3D reconstructed image of IGV: (a) upper view and (b) lower view. Black shaded area is the region where the prosthesis and master model is too close to be included in reconstruction.

C. Qualitative analysis

C-1. micro-CT analysis

Coronal, sagittal and horizontal CT cross sections of each printed and milled group were thoroughly examined under x20.5 magnification from the actual size. Since the platform position was the same during the CT scanning, the analysis was performed after arranging based on the bottom of the master model. Horizontal CT sections were selected from the AX area. The overall internal conformation differences between the groups were visually inspected and compared. The groups that presented specific repetitive features were recorded. The parts where specific differences appeared were observed in more in detail with SEM analysis.

C-2. Scanning electron microscope analysis

Internal surface of each printing specimen was imaged with SEM (Apreo S LoVac; Thermo Fisher Scientific, Brno, Czech) to investigate the tendency of microstructural differences with various printing conditions. Milling specimen was also taken for the comparison. The specimens were sputter coated with platinum (Q150T Sputter Coater; Quorum Technologies Ltd., Ashford, Kent, UK) and photographed under accelerating voltage of 15kV at magnifications of x60, x200, x500 and x1,000 for an inner occlusal surface and x100, x500 and x1,000 for an inner buccal surface.

Statistical analysis

For printed specimens (n=10 for ten groups), each value of AMD, MG, CE, AX, LA, OC and IGV was analyzed separately. All statistical analyses were performed with SPSS software (SPSS version 25; Chicago, IL, USA, IBM). The data were checked for normality with Shapiro-Wilk test and homogeneity of variance with Levene's test. Two-way analysis of variance (ANOVA) was conducted with two independent variables: the build orientation and layer thickness. When a statistical difference was observed, the following additional analyses were performed. One-way ANOVA was used to check the significance between the build orientations for each layer thickness, and independent t-test was used to check the significance between the layer thicknesses for each build orientation. One-way ANOVA was performed to compare the specific printed groups fabricated with desirable conditions and the milled groups for each AMD, MG, CE, AX, LA, OC and IGV independently. Post-hoc tests were performed using Tukey tests. The confidence level was set to a value of 95% (α = 0.05).

III. RESULTS

A. Quantitative results

A-1. Marginal fit of 3D printing

Marginal fit (AMD, MG) measured data are shown in Figure 14 (Table S1 in supplements). The smallest AMD was 71.9 ± 8.3 μm (50 μm, 45°) and the largest value was 121.6 ± 12.5 μm (50 μm, 90°). The effect on AMD of build orientation and layer thickness was checked with two-way ANOVA ($p < 0.001$). For 50 μm layer thickness groups, 0°, 30°, and 45° groups showed significantly smaller values than other groups. For 100 μm layer thickness groups, 30°, 45° and 60° groups showed significantly smaller values than other groups. The 50 μm layer thickness groups showed smaller values in 0° and 30° build orientations compared to the 100 μm groups. In contrast, the 100 μm layer thickness group showed a smaller value in the 60° build orientation compared to the 50 μm group.

The smallest MG was 41.6 ± 7.2μm (50 μm, 45°) and the largest value was 84.4 ± 12.3 μm (50 μm, 90°). The effect on MG of build orientation and layer thickness was checked with two-way ANOVA ($p = 0.002$). For 50 μm layer thickness groups, 0°, 30° and 45° groups showed significantly smaller values than other groups. For 100 μm layer thickness groups, the only a 90° group presented a significantly larger value than other groups. The 50 μm layer thickness groups showed smaller values in 0° and 45° build orientations compared to the 100 μm groups.

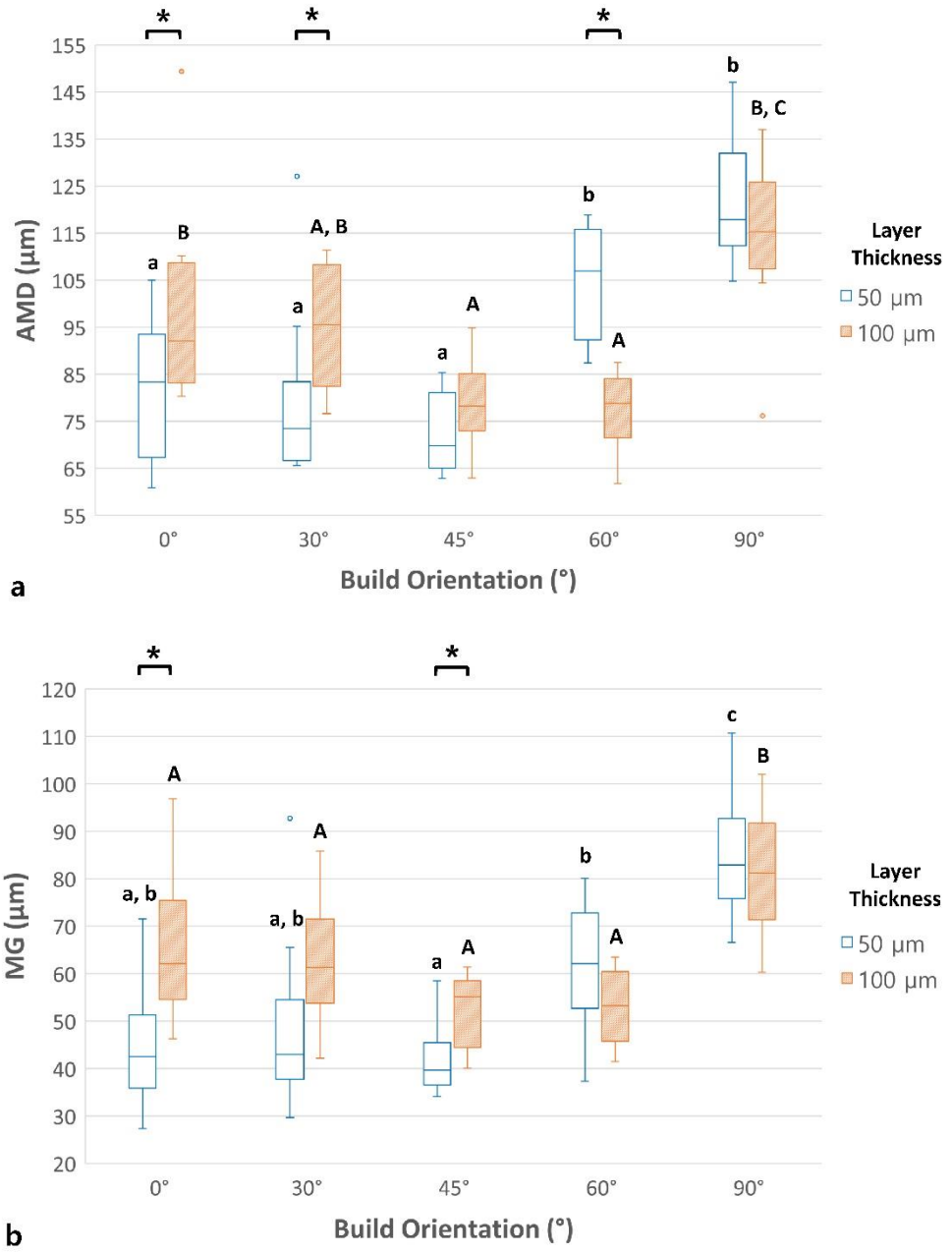

Figure 14. (a) Absolute marginal discrepancy (AMD) and (b) marginal gap (MG) of 3D printed prostheses. Different uppercase and lowercase letters indicate statistically significant differences in each layer thickness group. * indicates a statistically significant difference in each build orientation group.

A-2. Internal fit of 3D printing

A-2-1. Axial gap of 3D printing

Axial gap (CE and AX) measured data are shown in Figure 15 (Table S2 in supplements). The smallest CE was 67.1 ± 8.4 μm (50 μm, 60°) and the largest value was 122.1 ± 9.2 μm (50 μm, 0°). The effect on CE of build orientation and layer thickness was checked with two-way ANOVA ($p < 0.001$). For 50 μm layer thickness groups, the 60° group showed a significantly smaller value than other groups. For 100 μm layer thickness groups, the 45° and 60° groups showed significantly smaller values than other groups. The 50 μm layer thickness groups showed smaller values in 60° and 90° build orientations compared to the 100 μm groups. In contrast, the 100 μm layer thickness group showed a smaller value in the 0° build orientation compared to the 50 μm group.

The smallest AX was 79.0 ± 8.2 μm (50 μm, 60°) and the largest value was 115.0 ± 11.3 μm (50 μm, 0°). The effect on AX of build orientation and layer thickness was checked with two-way ANOVA ($p < 0.001$). For 50 μm layer thickness groups, 45°, 60° and 90° groups showed significantly smaller values than other groups. For 100 μm layer thickness groups, the 60° group showed a significantly smaller value than other groups. The 50 μm layer thickness groups showed smaller values (except at a 0° build orientation) compared to the 100 μm groups.

While investigating the coronal section, the inner AX (points h and o) and outer AX (points d and s) values had significant differences in 3D printed prostheses. For each

layer thickness, the inner AX (141.9 ± 23.7 μm for 50 μm, 172.3 ± 23.2 μm for 100 μm) was larger than the outer AX (92.7 ± 17.8 μm for 50 μm, 74.0 ± 16.6 μm for 100 μm) ($p < 0.001$ for each layer thickness). Investigating all conditions separately also showed the same trends. However, for milled prostheses, outer AX (93.0 ± 6.6 μm) and inner AX (96.9 ± 7.5 μm) were not significantly different ($p = 0.237$) (Fig. 16 (a)).

In the sagittal section, sagittal AX (points 4, 8, 15 and 19) values grossly decreased with a build orientation increase from 0° to 60° but increased in the 90° build orientation. For the 50 μm layer thickness, there was no significant difference between buccal AX and lingual AX except for the 90° group. Lingual AX was larger than the buccal AX in the 50 μm and 90° group ($p = 0.040$). For a 100 μm layer thickness, the buccal AX was larger than the lingual AX in the 0° group ($p = 0.008$). However, there was no significant difference in the 30° and 90° groups. Furthermore, lingual AX was larger than the buccal AX in the 45° and 60° groups ($p = 0.007$ and $p < 0.001$ respectively). For milled group, buccal AX (107.1 ± 17.8 μm) was larger than the lingual AX (89.7 ± 14.5 μm) ($p = 0.027$) (Fig. 16 (b)).

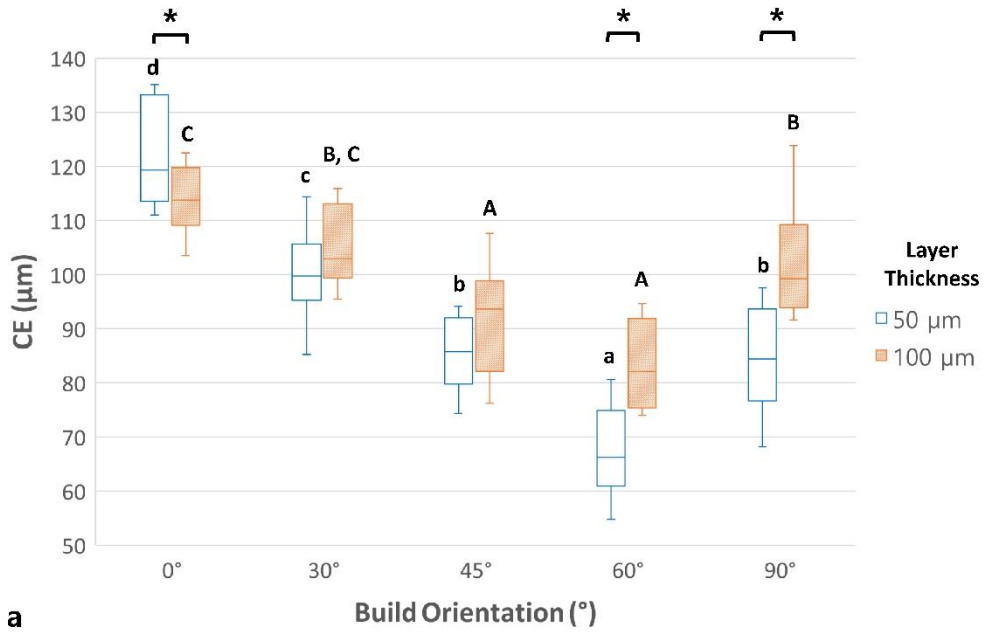

a

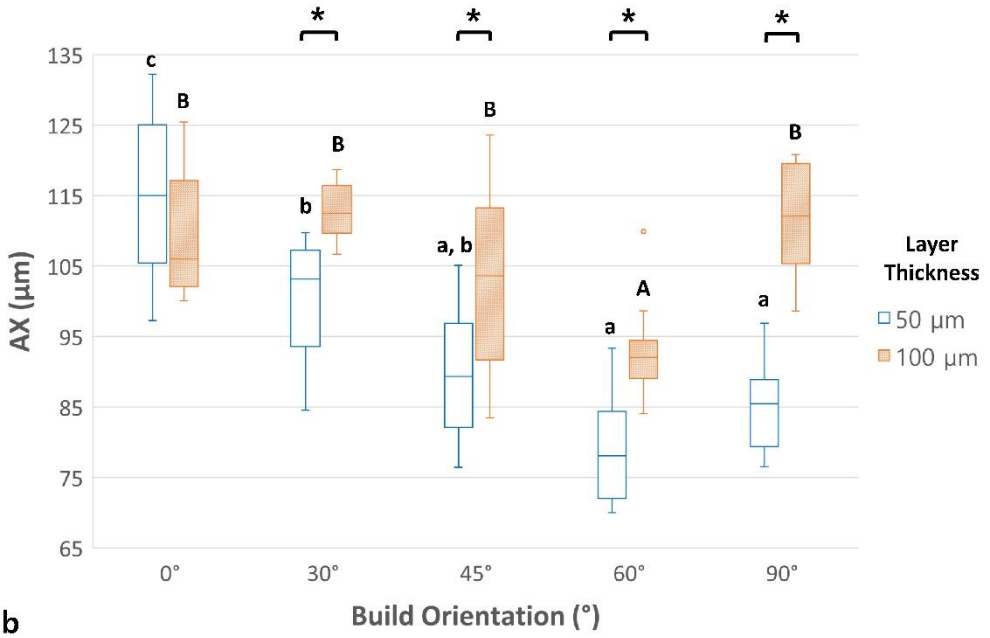

b

Figure 15. (a) Cervical area (CE) and (b) mid axial wall area (AX) of 3D printed prostheses. Different uppercase and lowercase letters indicate statistically significant differences in each layer thickness group. * indicates a statistically significant difference in each build orientation group.

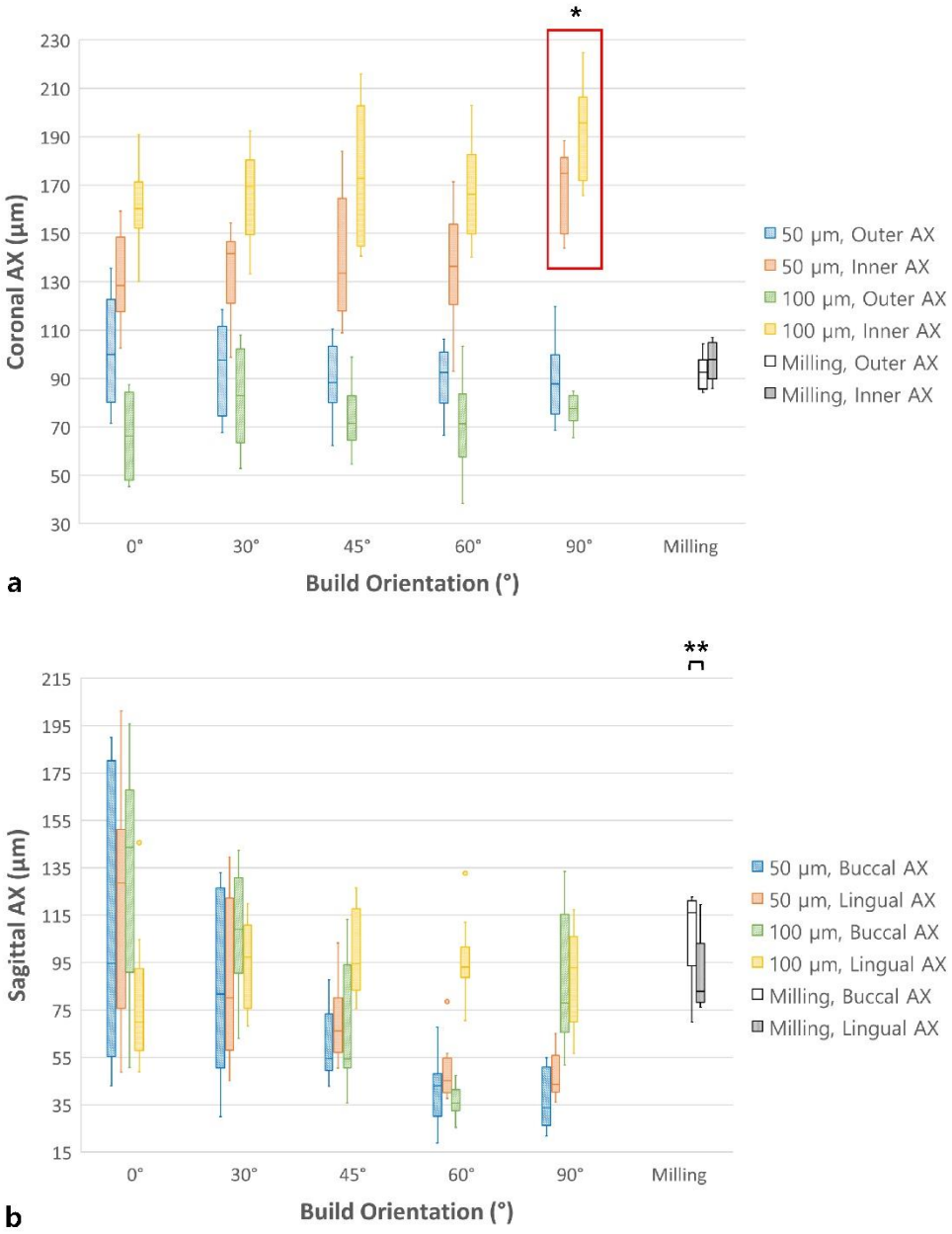

Figure 16. (a) Coronal AX of 3D printed and milled prostheses. * indicates that the inner AX of 90° groups was larger than the other build orientation groups. (b) Sagittal AX of 3D printed and milled prostheses. ** indicates significant difference between the buccal and lingual AX in milled group.

A-2-2. Occlusal gap of 3D printing

Occlusal gap (LA and OC) measured data are shown in Figure 17 (Table S3 in supplements). The smallest LA was 65.7 ± 6.5 μm (100 μm, 90°) and the largest value was 102.3 ± 8.0 μm (100 μm, 30°). The effect on LA of build orientation and layer thickness was checked with two-way ANOVA ($p < 0.001$). For 50 μm layer thickness groups, no statistical difference was observed with changes in build orientation ($p = 0.057$). For the 100 μm layer thickness groups, the 90° group showed a significantly smaller value than other groups. The 50 μm layer thickness groups showed smaller values in 0°, 30° and 45° build orientations compared to the 100 μm groups.

The smallest OC was 97.4 ± 25.5 μm (50 μm, 30°) and the largest value was 206.0 ± 16.7 μm (100 μm, 0°). The effect on OC of build orientation and layer thickness was checked with two-way ANOVA ($p < 0.001$). For 50 μm layer thickness groups, the 0° and 30° groups showed significantly smaller values than other groups. For the 100 μm layer thickness groups, 45°, 60° and 90° groups showed significantly smaller values than other groups. The 50 μm layer thickness groups showed smaller values in 0°, 30° and 45° build orientations compared to the 100 μm groups. In contrast, 100 μm layer thickness group showed smaller values in the 90° build orientation compared to the 50 μm group.

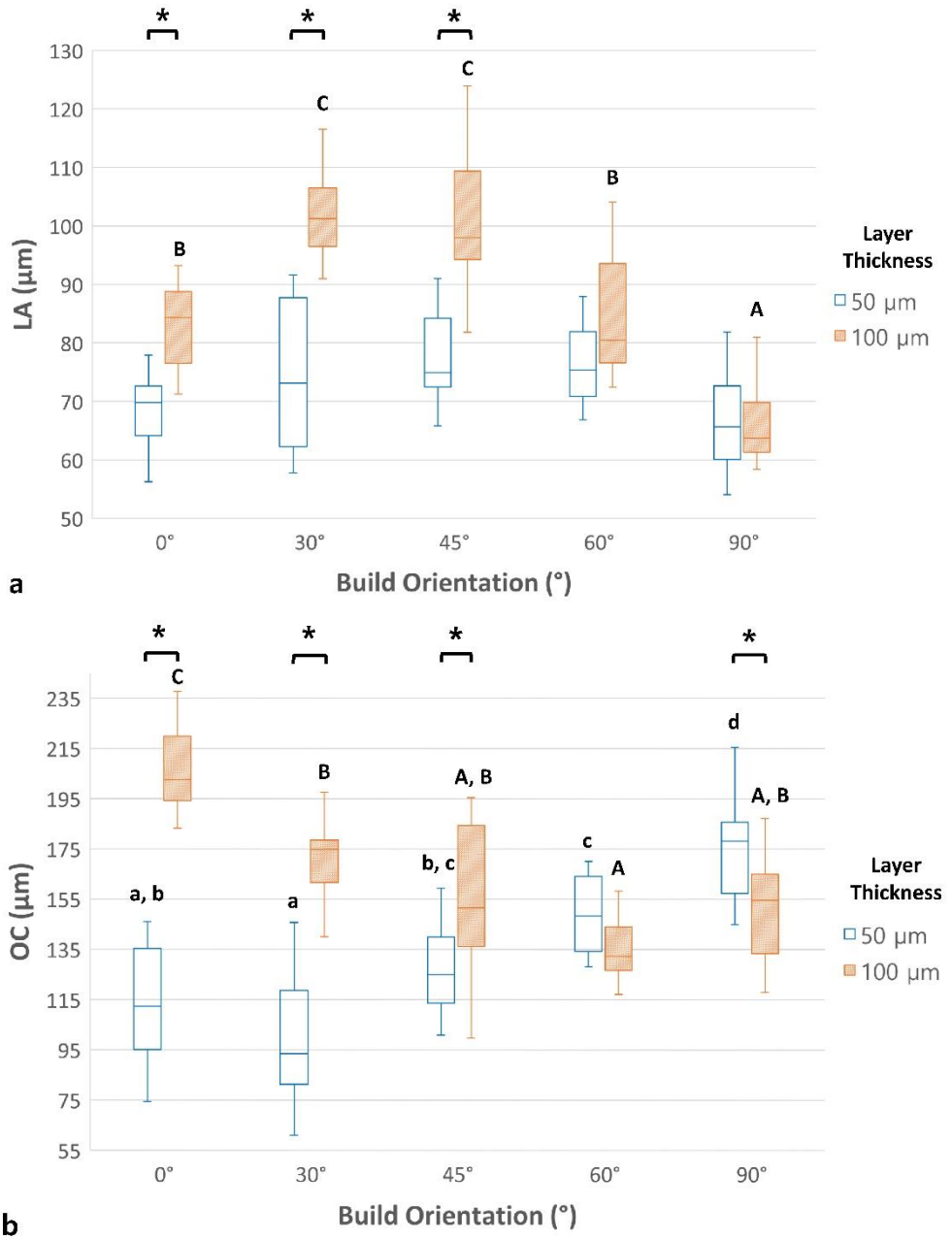

Figure 17. (a) Line-angle area (LA) and (b) occlusal area (OC) of 3D printed prostheses. Different uppercase and lowercase letters indicate statistically significant differences in each layer thickness group. * indicates a statistically significant difference in each build orientation group.

A-3. Internal gap volume of 3D printing

Internal gap volume (IGV) measured data are shown in Figure 18 (Table S4 in supplements). The smallest IGV was 20.2 ± 1.2 mm^3 (50 μm, 60°) and the largest volume was 25.5 ± 1.3 mm^3 (100 μm, 30°). Both build orientation and layer thickness had effects on the IGV ($p < 0.001$ for both independent variables). For 50 μm layer thickness groups, 45° and 60° groups showed significantly smaller values than other groups. For 100 μm groups, the 60° group showed a significantly smaller value than other groups. Except for the 0° build orientation, 50 μm groups showed smaller values than the 100 μm groups for each build orientation.

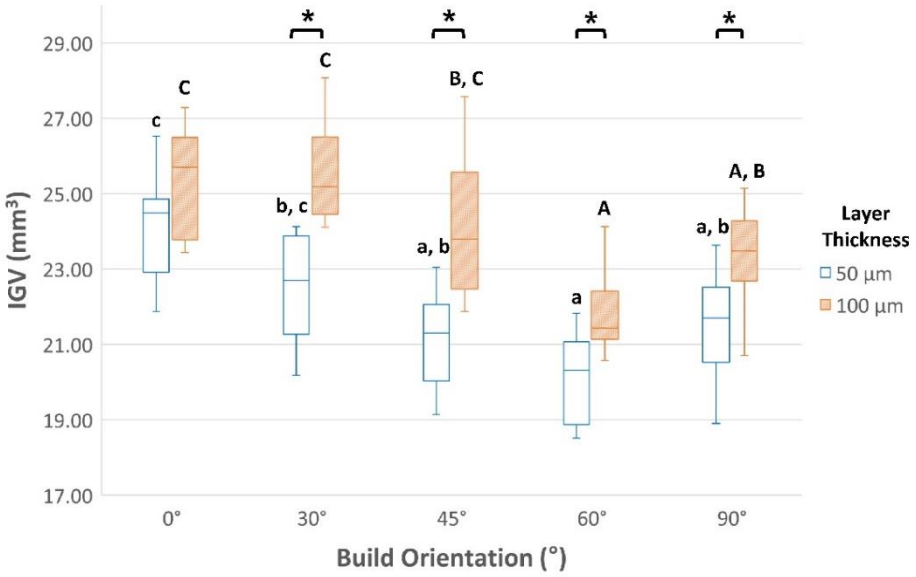

Figure 18. Internal gap volume (IGV) of 3D printed prostheses. Different uppercase and lowercase letters indicate statistically significant differences in each layer thickness group. * indicates a statistically significant difference in each build orientation group.

A-4. Comparison of 3D printing and milling

From the results above, the desirable conditions for fabricating the prostheses with adequate marginal and internal fit could be deduced with 45° or 60° build orientations in a 50 μm layer thickness. Therefore, IGV, AMD, MG, CE, AX, LA and OC data were plotted as shown in Figure 19 (Table S5 in supplements) compared with milled prostheses data. The AMD and CE of 3D printed groups were significantly smaller than those of the milled group ($p < 0.001$ for both). However, the MG and LA of the 3D printed groups were significantly larger than those of the milled group ($p < 0.001$ for both). For IGV, statistical difference was found only between 50 μm, 45° 3D printed group and milling. Milled group showed smaller IGV compare to 50 μm, 45° 3D printed group. For AX, statistical difference was found only between 50 μm, 60° 3D printed group and milling. 3D printed group with 50 μm, 60° conditions showed smaller AX compare to milled group. For OC, only difference was found between the 3D printed groups.

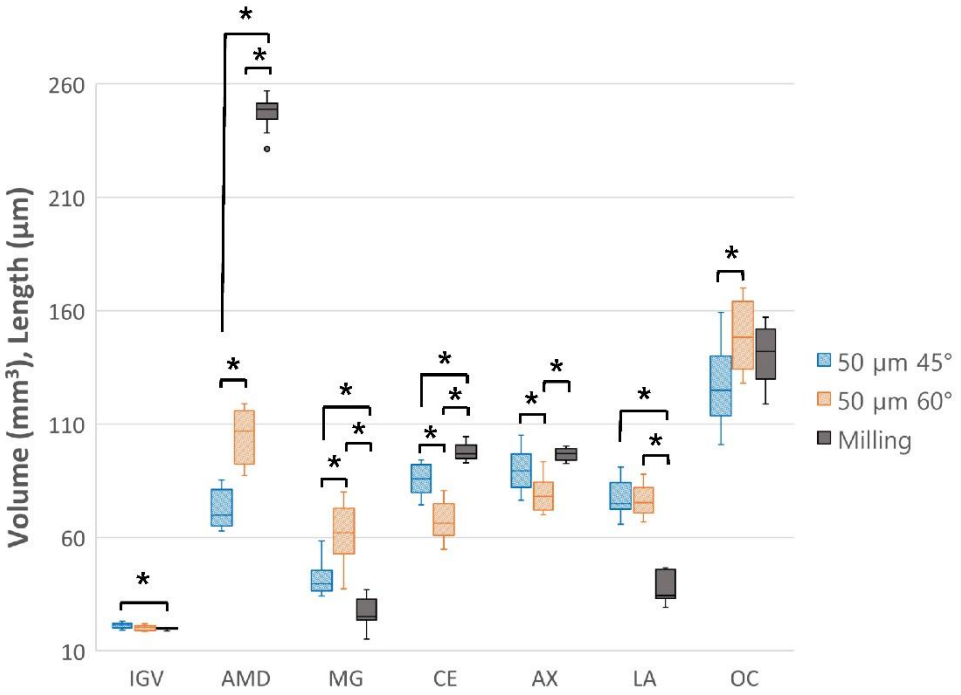

Figure 19. Comparison of the internal gap volume (IGV), marginal fit (AMD, MG), internal fit (CE, AX, LA, OC) between the 3D printed and milled prostheses. * indicates statistically significant difference between the groups. The AMD and CE were significantly smaller in the 3D printed groups. The MG and LA were significantly smaller in the milled group.

B. Qualitative results

B-1. Characteristic findings on micro-CT

A stair-shaped appearance was observed for all printed groups. This shape was absent in milled groups (Fig. 20) and appeared more prominently in 100 μm groups than 50 μm groups.

From the quantitative results, inner AX was larger than the outer AX in the printed groups. No such characteristic was observed in the milled group. This fact could be observed more intuitively in the horizontal CT section. In Figure 21, it can be confirmed that the inner AX was larger than the outer AX for the printed groups. In contrast, inner and outer AX seemed equal for the milled group from the horizontal CT section. In addition, a more uniform cement space could be observed in milled group compare to the printed groups (Fig. 21 (d)).

In Sagittal CT section, there was no characteristic differences among the 30°, 45° and 60° printed groups. However, irregular inner occlusal surface was observed in 0° groups regardless of the layer thickness. For 90° groups, large wavy and uneven surface patterns on the inner buccal surface were observed (Fig. 22). This pattern appeared more prominently in 100 μm groups than 50 μm groups.

Since the surface configuration was different among the groups, internal surfaces of the specimens were examined more in detail with SEM analysis.

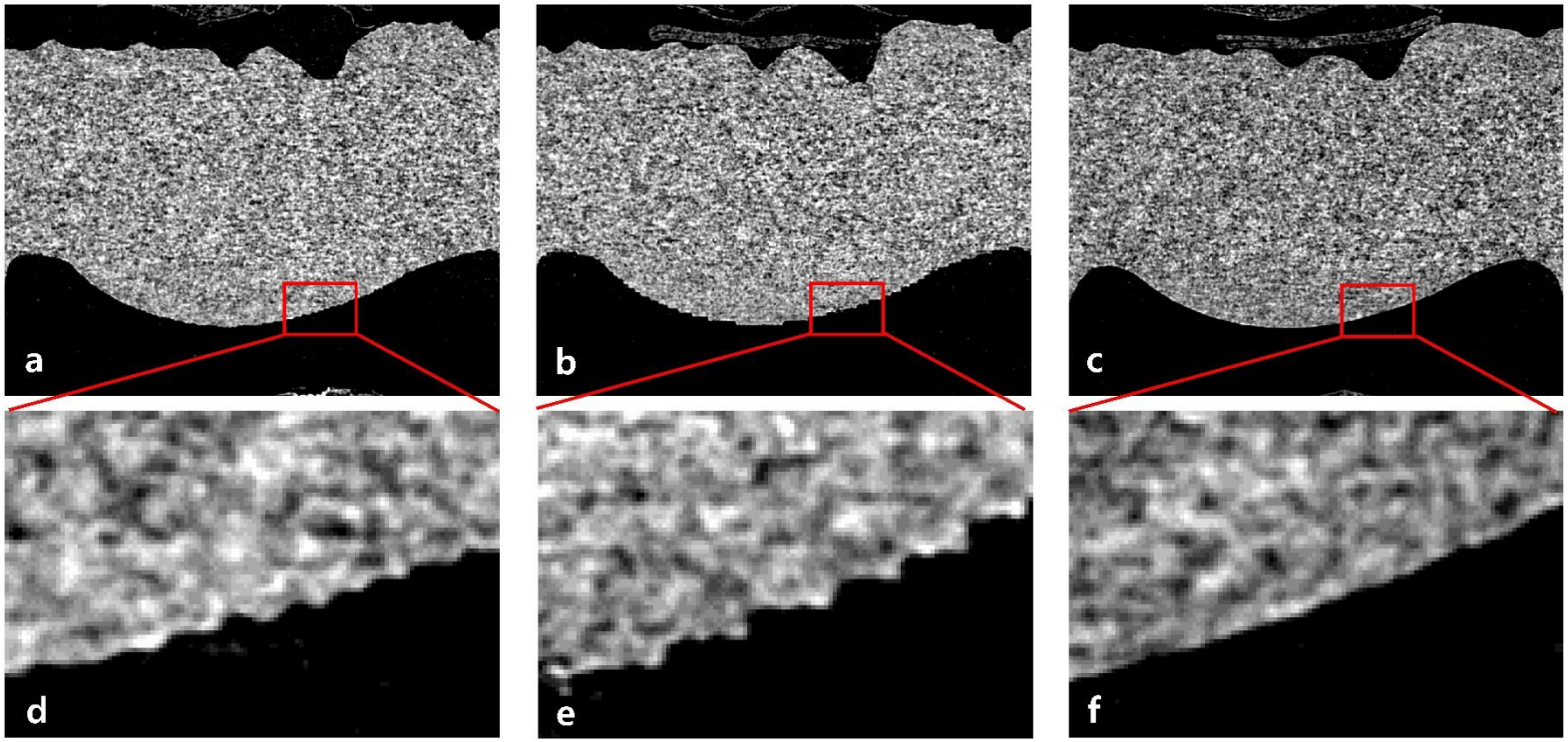

Figure 20. Coronal CT section at the pontic area. (a) Printed (50 μm, 0°), (b) printed (100 μm, 0°), (c) milled group, (d) enlarged view of red box area in (a), (e) enlarged view of red box area in (b), (f) enlarged view of red box area in (c). Stair-shaped appearance was observed in printed groups only. This shape appears more prominently in layer thickness of 100 μm rather than 50 μm.

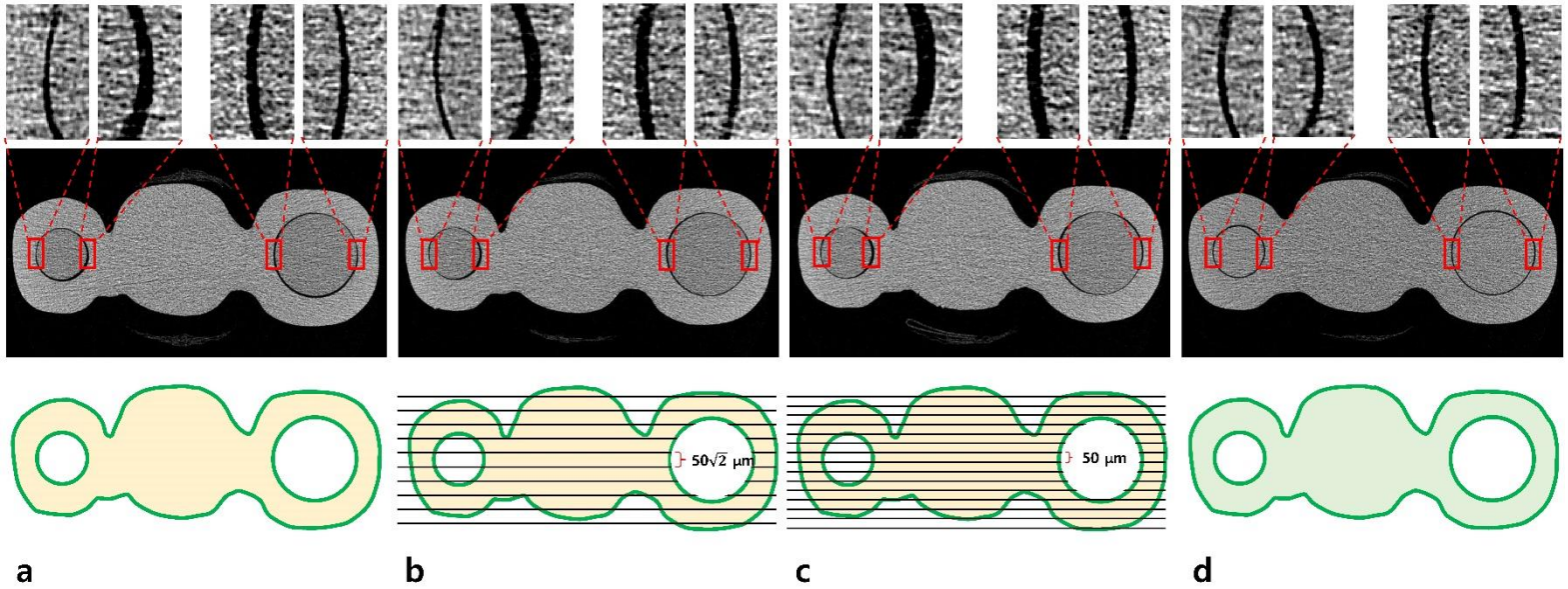

Figure 21. Horizontal CT section at the AX area. (a) Printed (50 μm, 0°), (b) printed (50 μm, 45°), (c) printed (50 μm, 90°), and (d) milled group. Inner AX > Outer AX for all printing specimens. As the build orientation increases, the number of build layers consisting the horizontal cross section increase and the thickness of each build layer decreases simultaneously. From (a), single build layer consists whole AX cross section. From (b), single build layer thickness becomes $50\sqrt{2}$ μm. From (c), single build layer thickness becomes 50 μm. More uniform cement space was observed in (d) milled group compared to the (a), (b), (c) printed groups.

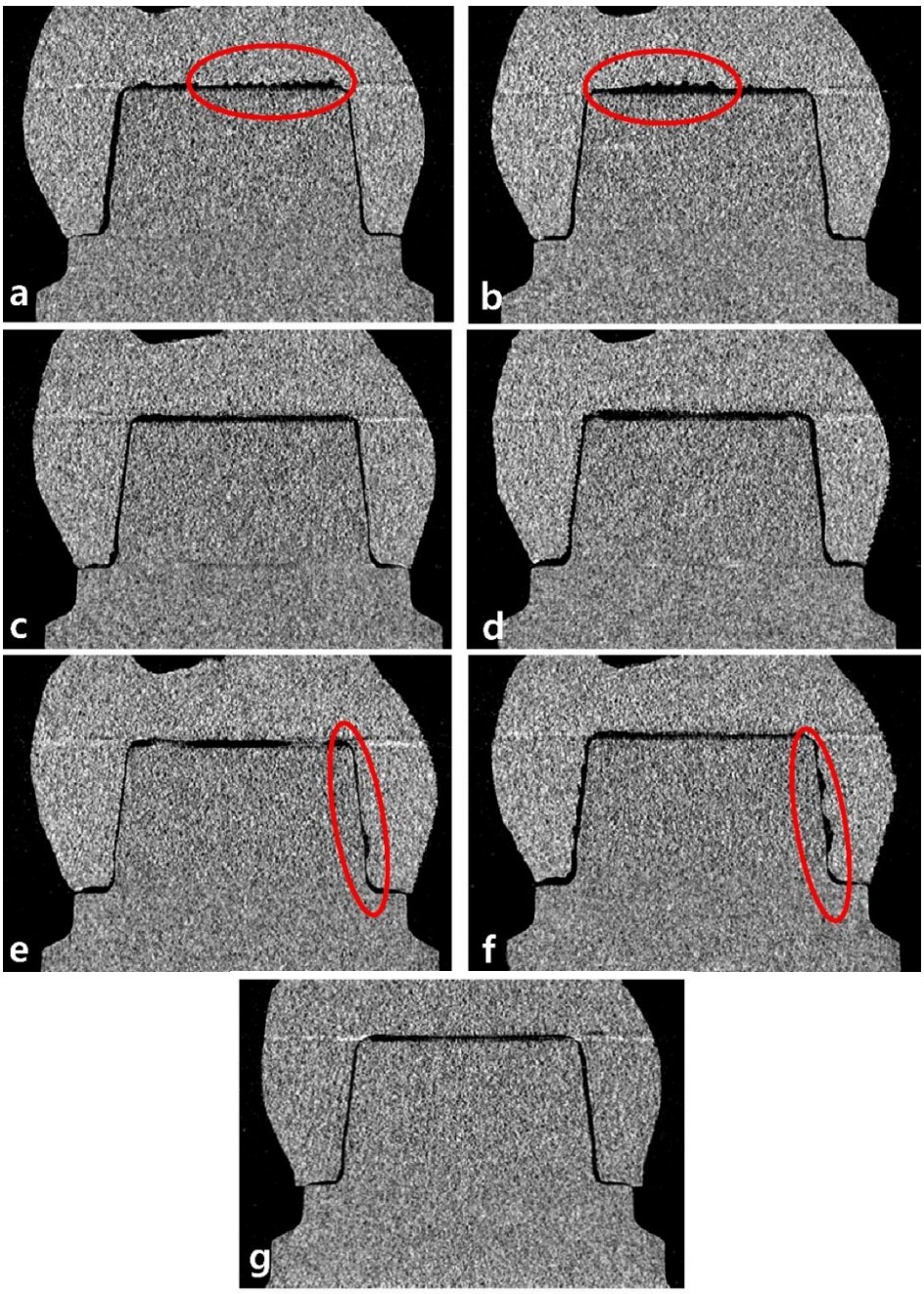

Figure 22. Sagittal CT sections at the molar area. (a) printed (50 µm, 0°), (b) printed (100 µm, 0°), (c) printed (50 µm, 45°), (d) printed (100 µm, 45°), (e) printed (50 µm, 90°), (f) printed (100 µm, 90°), and (g) milled group. Red circles emphasize the characteristic findings on the inner surface of the printed prostheses.

B-2. Characteristic findings on scanning electron microscope

The SEM images of the internal surface of molar area are shown in Figure 23 and 24. The difference in internal surface pattern was observed according to the printing conditions. As the layer thickness decreases, it is clearly observed that the smoother surface was presented. Red arrows of Figure 23 (a) and (b) present that some part of the inner occlusal surface was partially missing and incompletely manufactured. Thus, the voids could be seen on the inner occlusal surface. In the case of the 30°, 45°, 60° specimens, minor polymerization error such as the red arrow indication in Figure 23 (e) and (h) may occur, but a relatively uniform surface was observed compare to other build orientations. In the case of the 60° specimens, small flaws were sparsely observed which were limited in single build layer (Fig. 23 (h)). In the case of the 90° specimens, considering actual layering pattern, horizontal lines should be observed but the vertical lines were observed instead (red arrow of Fig. 23 (i)). When the layering continues on the missing area, self-supported structure is not satisfied. Those polymerization error can accumulate on the multiple build layers. Thus, it can be seen as the vertical flaw (red arrow of Fig. 23 (j)).

Red arrows of the Figure 24 (a) and (b) indicate the small vertical lines which were created as a same manner in Figure 23 (i) and (j). From Figure 24 (i) and (j), large voids on the inner buccal surface of 90° condition were observed. The size of the void was larger in 100 μm layer thickness groups compare to the 50 μm groups.

Surface smoothness was better for milling specimens compared with all printed specimens.

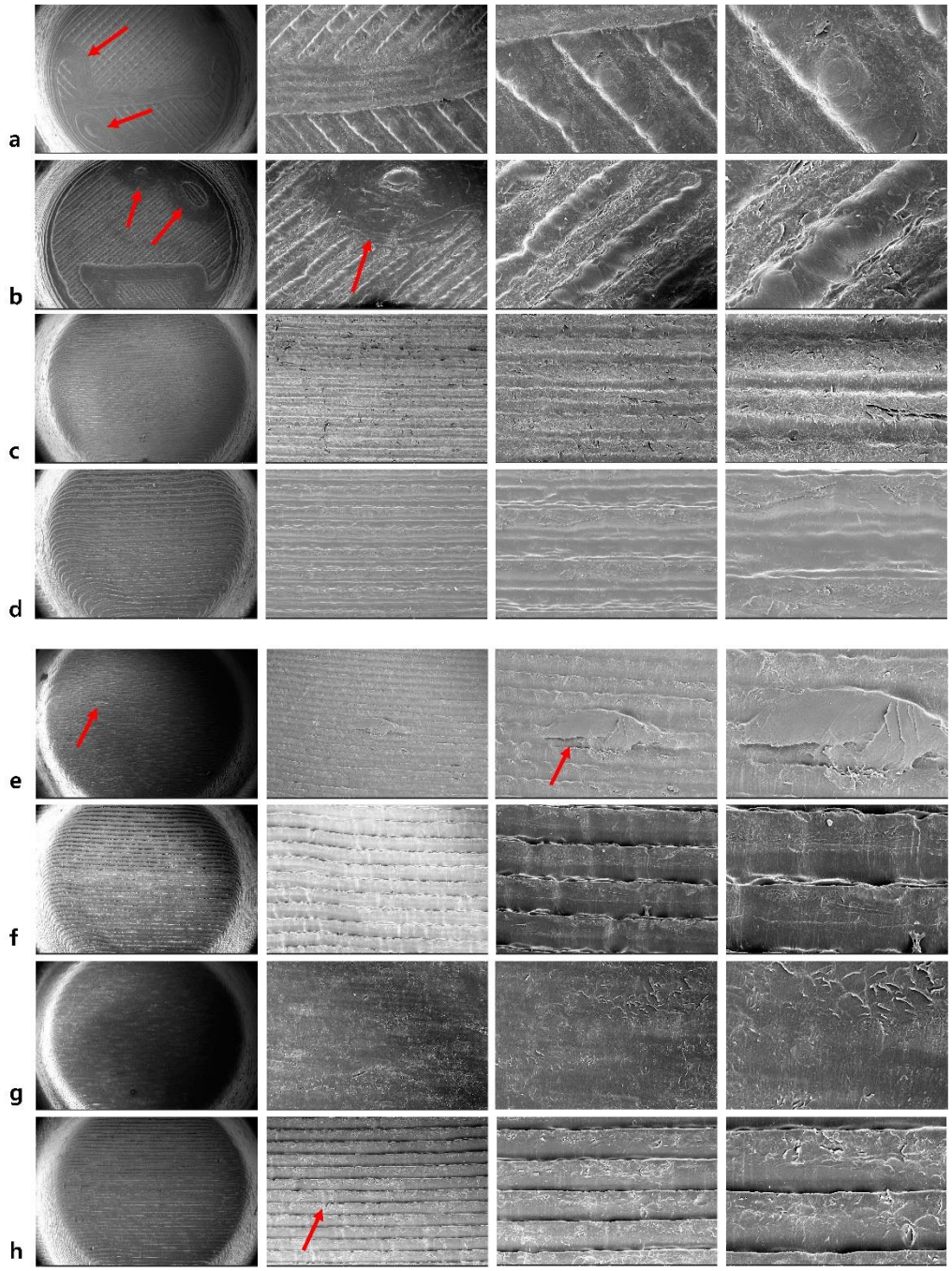
a
b
c
d
e
f
g
h

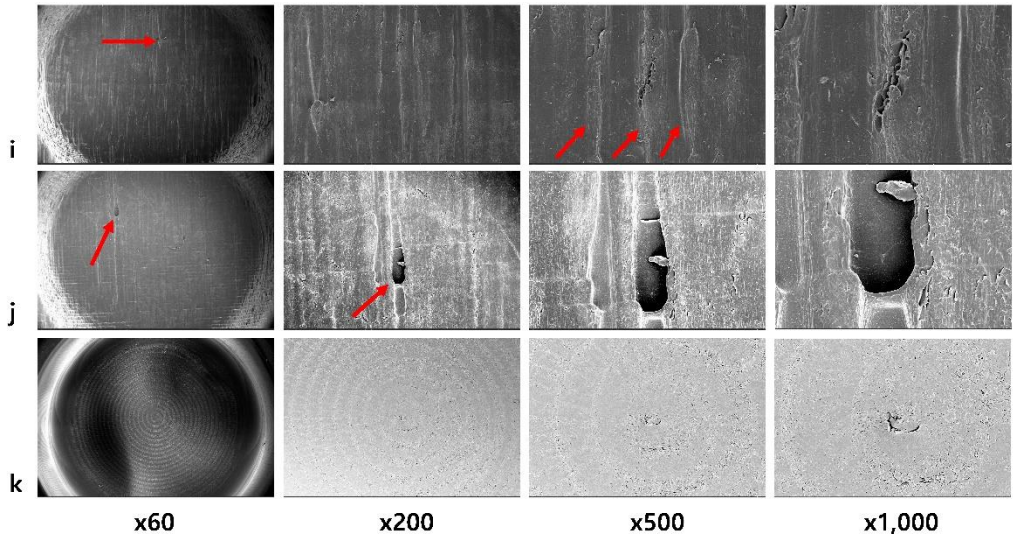

Figure 23. SEM images of the inner occlusal surface. (a) printed (50 µm, 0°), (b) printed (100 µm, 0°), (c) printed (50 µm, 30°), (d) printed (100 µm, 30°), (e) printed (50 µm, 45°), (f) printed (100 µm, 45°), (g) printed (50 µm, 60°), (h) printed (100 µm, 60°), (i) printed (50 µm, 90°), (j) printed (100 µm, 90°), and (k) milled group. Red arrows in (a) and (b) indicate the voids. Red arrows in (e) and (h) indicate the minor polymerization error. Red arrows in (i) indicate vertical lines. Red arrows in (j) indicate the vertical flaw.

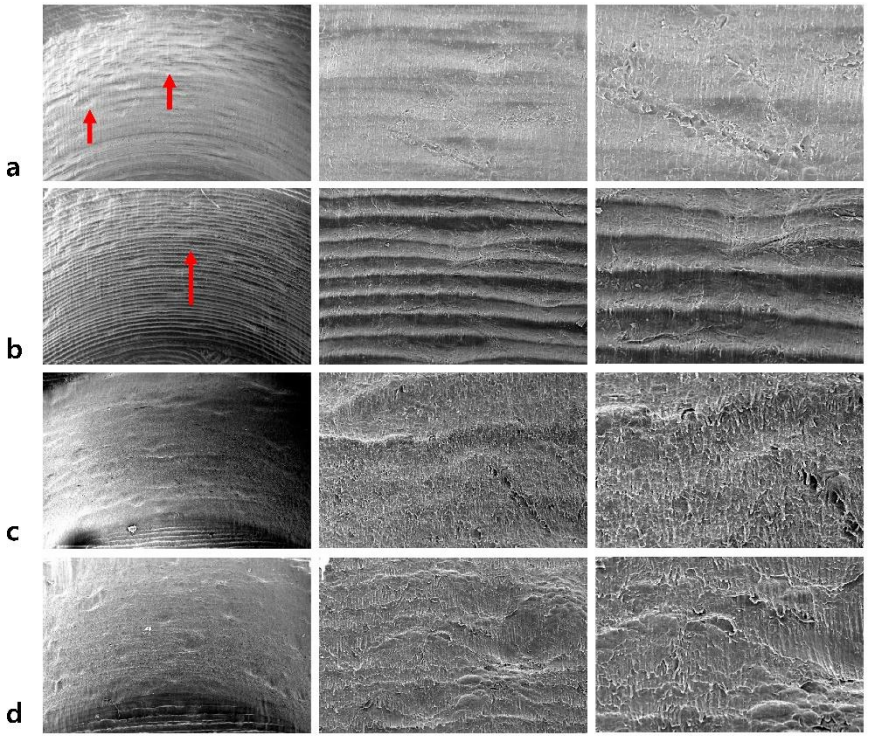
a
b
c
d

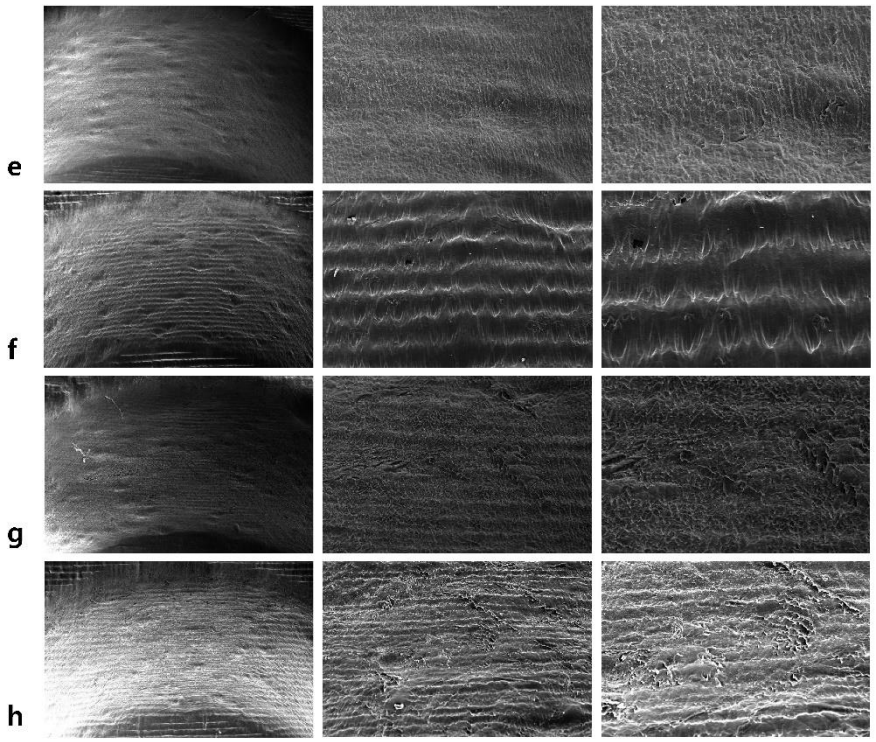
e
f
g
h

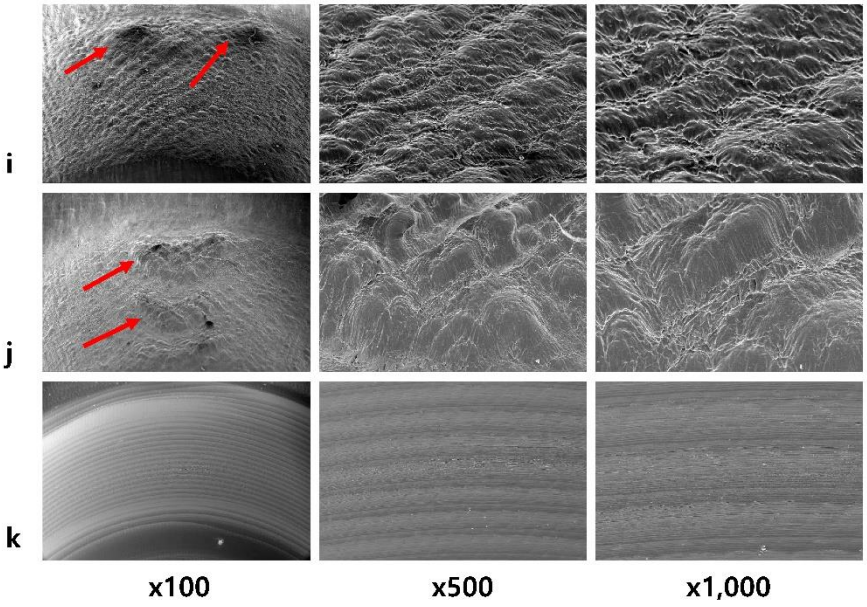

Figure 24. SEM images of the inner buccal surface. (a) printed (50 µm, 0°), (b) printed (100 µm, 0°), (c) printed (50 µm, 30°), (d) printed (100 µm, 30°), (e) printed (50 µm, 45°), (f) printed (100 µm, 45°), (g) printed (50 µm, 60°), (h) printed (100 µm, 60°), (i) printed (50 µm, 90°), (j) printed (100 µm, 90°), and (k) milled group. Red arrows in (a) and (b) indicate the small vertical lines. Red arrows in (i) and (j) indicate the large voids.

IV. DISCUSSION

The present study analyzed the marginal and internal fit of three-unit resin prostheses manufactured by SLA 3D printing according to the build orientation and layer thickness and compared them with milled prostheses. All null hypotheses were rejected as the build orientation and layer thickness affected the marginal and internal fit, and there were differences due to the manufacturing methods – milling or SLA 3D printing.

When additive manufacturing begins, Hu[46] stated that STL file is sliced and changes to the G-code, a type of computer numerical control programming language. When original STL data are converted to the G-code, more inaccurate data gather if large layer thickness had applied. If the layer thickness decreases, more precise structures can be manufactured. This was also confirmed in the present study. Preferable marginal and internal fits were observed when the layer thickness was 50 μm than when it was 100 μm.

Build orientation also plays an important role in this process because the single layer shape can vary according to the build direction. Figure 21 (a) shows the AX cross-cut image of 0° build orientation which is consisted by a single build layer. CAD data loss could occur at cross sectional border area. As the build orientation increases, AX cross-cut is consisted by multiple numbers of layers (Fig. 21 (b) and (c)). Accordingly, more precise result in horizontal section derived, resulting the smaller AX value until increase to 60°. One of the reason was that there are many chances that can compensate the data loss. However, increase the build orientation to 90° is not recommended

because self-supporting structure is not satisfied.

The build layers are polymerized one after another. In this process, polymerization shrinkage can affect the prosthesis. Shrinkage has an exponential relationship with the layer thickness.[47] The shrinkage occurs in the inward direction.[48] Ishida and Miyasaka[49] reported that most single crowns manufactured by additive manufacturing methods showed reduced diameters compared to the original CAD data. In this study, the amount of shrinkage seems to occur inward to the pontic area regardless of the build orientation, resulting in the outer/inner AX difference (Fig. 16 (a) and Fig. 21 (a), (b) and (c)). As the build orientation increase, more supporters attach to the lingual surface than to the occlusal surface. The lingual AX tends to be larger than the buccal AX until 60° for 100 μm layer thickness groups (Fig. 16 (b)). Therefore, it can be cautiously interpreted that the shrinkage may occur parallel to the build direction.

A self-supporting structure is important for the dimensional accuracy of a 3D printed product. Alharbi et al.[40] reported that a 120° (60° in this study) build orientation was recommended from the perspective of the dimensional accuracy and time needed for finishing the SLA printed prosthesis. They reported that the self-supported surface may change depending on the build orientation and recommended attaching supports where the angle is less than 45° between the tangent line of the structure surface and x-y plane. In the present study, the supports were sufficiently attached when printing the lingual surface in 90° groups. However, when printing the buccal surface, it seems that the previous layer itself could not serve the role of a support for the next build layer due to the sudden build layer area change. Therefore, unsupported resin can be washed out, resulting in voids on the buccal inner surface (Fig. 24 (i) and (j)) which was

unintentionally occurred during the manufacturing (Fig. 22 (e) and (f)).

All printed specimens had a stair-shaped appearance (Fig. 20). This shape became more prominent as the layer thickness increased in this study. Zhai et al.[50] discussed about this phenomenon with laser power difference. They suggested that increasing laser power leads surface roughness increase. Ligon et al.[51] also mentioned about this phenomenon as a 'stair step' surface. Yang et al.[52] also stated that stair shape is inevitable for SLA additive manufacturing and reported that build orientation can affect the surface roughness of the printing result. This shape can mainly be seen in photopolymer 3D printed prosthesis and is a unique characteristic. Since the layer thicknesses were 50 μm and 100 μm in this study, the stair-shaped appearance might affect the prosthesis fit because the ranges of the marginal and internal fit were 41.6 μm (MG; 50 μm, 45°) – 206.0 μm (OC; 100 μm, 0°), respectively.

Laser irradiation time can also affect the fit.[51] Choosing a layer thickness of 100 μm requires a longer irradiation time to complete the polymerization at a point. That is, additional polymerization may occur in the x- and y- directions at the outermost area of a single build layer compared to the 50 μm layer thickness condition. Considering this factor, the smaller gaps presented by the 100 μm groups can be explained: 60° groups in AMD, 0° groups in CE and 90° groups in OC. For CE, x- and y- axis elements have more influence in the 0° build orientation groups. For OC, x- and y- axis elements have more influence in the 90° build orientation groups. Since the AMD represents the horizontal and vertical discrepancy, x- and y- axis elements are effective in all build orientations.

Five factors are important in SLA 3D printing: (1) G-code data processing, (2) polymerization shrinkage, (3) self-supporting structure, (4) stair-shaped appearance and (5) laser irradiation time. Combined interactively with (1) build orientation and (2) layer thickness, seven factors seem to have an effect on the prosthesis fit (AMD, MG, CE, AX, LA, OC and IGV). Studies such as Tahayeri et al.[39] showed that even a simple form of prosthesis can undergo dimensional changes and that z-axis elements had high accuracy. In the case of the complex form of prosthesis as in this study, the actual crown morphology, it can be said that the dimensional change occurs as a complex manner. Three-dimensional change of the prostheses could not be numerically standardized in this study. Further studies will be needed for more exact interpretations.

Maximum clinically acceptable marginal discrepancy values have been reported varying from 50 to 200 μm.[53-56] As such, there is no clear consensus. However, it is obvious that the minimal marginal and internal discrepancy is clinically important.

In the marginal fit analysis, there was no significant difference due to the build orientation when the build orientation was less than 45°, but differences due to the layer thickness were found. AMD and MG values of the 50 μm groups were lower than that of the 100 μm groups. For 50 μm groups, marginal gap values significantly increased as the build orientation increased by above 45°, showing a maximum at 90°. For 100 μm groups, the maximum value was also observed at 90°. X-, y- and z-axis elements may vary according to the build orientation. Up to a 45° build orientation, the z-axis elements are closely related to the MG, resulting in smaller marginal gaps. According to these results, choosing a 50 μm layer thickness and setting the build orientation to 45° may help to get a proper marginal fit for 3D printed prostheses.

Boitelle et al.[57] reported 9-206.3 μm of AMD in CAD/CAM fabricated bridge framework. In this study, the AMD value was 71.9-121.6 μm which is in the range of a past study. Mclean and Fraunhofer[53] suggested that a marginal discrepancy up to 120 μm is acceptable in clinical applications. Petteno et al.[7] suggested that the clinically acceptable marginal gap for a cast prosthesis is up to 70 μm. In this study, the MG value was 41.6-84.4 μm. Except for the 90° build orientation groups, the largest MG value was 66.1 μm. Therefore, a 90° build orientation seems undesirable, which may increase the marginal gap.

As the build orientation increased from 0° to 60°, and when the layer thickness was thinner, IGV and axial gaps (CE, AX) tended to decrease (Fig. 15 and 18). However, the axial gaps (CE, AX) increased significantly when the build orientation increase to 90°. In the axial gap analysis, both CE and AX graph showed similar pattern without distinction of coronal/sagittal value. An axial cement thickness beyond 122 μm is not clinically recommended because it can reduce the fracture resistance of the crown.[59] Increased axial cement thickness may reduce the crown retention.[60] Build orientations of 0° and 90° are not desirable because some specimens presented large axial gaps (Fig. 15). Therefore, build orientations over 60° are not recommended, a conclusion which is similar to past research.[41] Most of the groups showed smaller axial gap values in 50 μm layer thickness compare to 100 μm.

In the occlusal gap analysis, LA and OC values showed different tendency with build orientations and layer thickness variables. The graph of LA seems to be symmetrical: LA increases as the build orientation increases to 45° and decreases after that (Fig. 17 (a)). It can be assumed that the stacking pattern of the resin layer had an

effect on this result. Figure 25 clearly shows that the stacking pattern differs depending on the build orientations.[50,60]

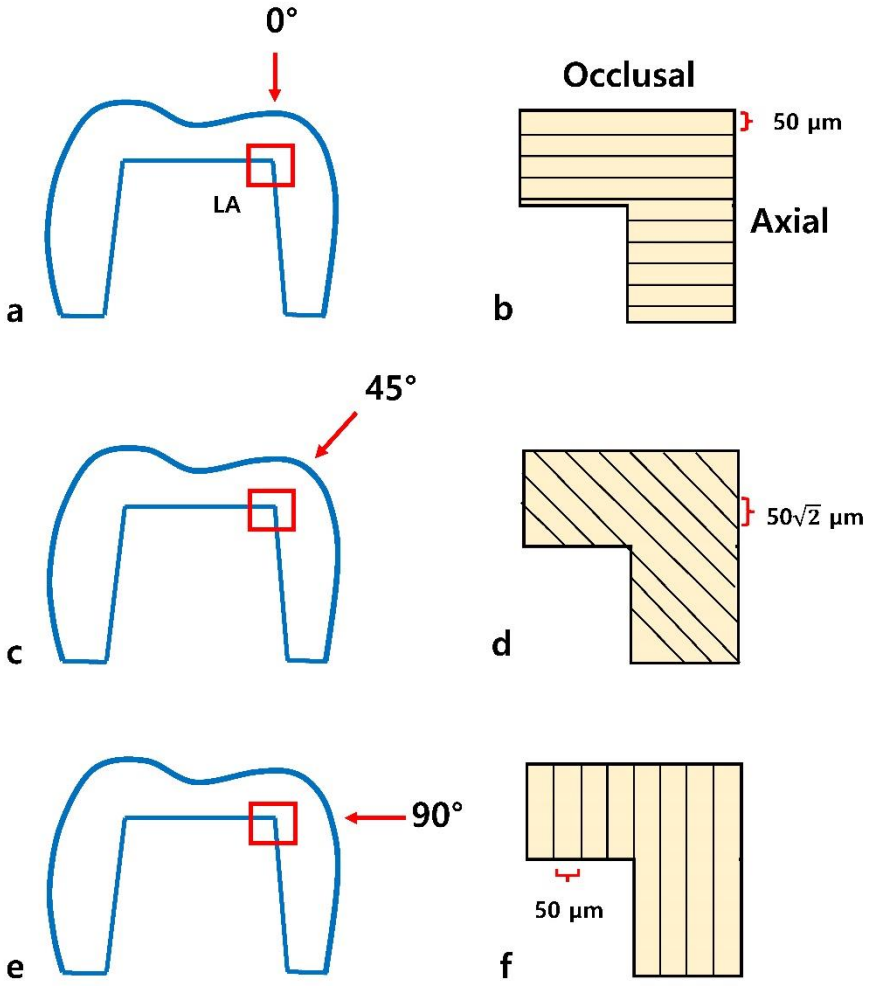

Figure 25. Enlarged diagram with resin stacking pattern at sagittal LA area. (a) printed (50 µm, 0°), (b) enlarged diagram of red box area in (a), (c) printed (50 µm, 45°), (d) enlarged diagram of red box area in (c), (e) printed (50 µm, 90°), (f) enlarged diagram of red box area in (e). Same stacking thickness (50 µm) was applied for (b) and (f). On the other hand, (d) was manufactured with stacking thickness of $50\sqrt{2}$ µm.

In terms of the OC results, Figure 17 (b) shows the large discrepancy in values between 50 μm and 100 μm layer thicknesses for 0° and 30° build orientations. This result seems natural considering the G-code data processing.

IGV values of 3D printed prostheses were 20.2-25.5 mm^3 in this study. Yildirim et al.[61] and Kim et al.[62] found that the IGVs for clinically acceptable lithium disilicate single crowns were 12.6-18.2 mm^3, and 25.3-40.7 mm^3, respectively. Considering that 3-unit prostheses were investigated in this study, it can be interpreted that the 3D printed prostheses exhibited clinically acceptable IGV values.

The quantitative results could be visually confirmed with SEM observation. Figure 23 (a) and (b) clearly shows the voids which leads to increase OC value. Figure 23 and 24 shows that the inner surfaces of 30°, 45°, 60° build orientation are more uniform and had less flaws compare to 0° and 90°. In all cases, a layer thickness of 50 μm was preferable to 100 μm on perspective of the surface smoothness. Shim et al.[63] also reported similar surface characteristics according to the 0°, 45°, 90° build orientation. Figure 23 (i) and (j) shows lines and flaws parallel to the layering direction. Hague et al.[64] also presented the SLA rapid prototyping model with parallel lines to the build direction. These lines are presumed to form by the flow of unpolymerized resin on the surface, which are inherent drawback of vat polymerizing additive manufacturing. If the polymerization is not completely carried out in the previous x-y plane and the next layer starts to polymerize, a continuous flaw may be created.

. Such characteristics were not found in the milled group. This suggests that the inner surface configuration could be affected by the manufacturing method, even if the

same CAD data were used. From these, additional manufacturing which can cause a change in three-dimensional configuration, can be seen as an inferior method compared to subtractive manufacturing. However, the milled group showed very large AMD values with an over-extended margin despite following the manufacturer's instructions. In contrast, MG values were smaller in milled groups. Inherent manufacturing error of 3D-printing might be the one of the reasons. CE was larger and LA was smaller in the milled group. The milling bur shapes and accessibility could affect this result. LA area is hard to cut down precisely with blunt-ended milling burs.

Although the prosthesis fits were different among the printed groups, most groups had clinically acceptable fits. Both printed and milled groups presented clinically acceptable ranges.[25]

Park et al.[34] conducted a similar study with a DLP 3D printer. In that study, 45° and 60° build orientations with a 100 μm layer thickness showed a smaller marginal gap. In the present study, the results for build orientation were consistent. However, the results for the layer thickness were contradictory, in that smaller AMD and MG values were achieved with the 50 μm layer thickness. This disagreement might have originated from the difference between the DLP and SLA printing processes and prosthesis design. Compared with the previous study, the present study performed inner/outer/buccal/lingual AX analysis with qualitative analysis in addition. Therefore, the effect of printing conditions on fit could be interpreted in more detail.

The internal fit can be measured in various ways.[25] The most commonly used method is direct cross-sectioning. It has a drawback that cross-sectioning may cause

deformation due to the applied external force. Moreover, since the specimens are destroyed, only a limited number of cross-sectional planes can be made.[25,65]

Therefore, the replica method can be used. Using the silicon light body impression materials, a replica of the cement space can be obtained. This replica is sectioned and used to measure the internal gap value through a microscope. However, if the thickness at the measuring point is too shallow, the measurement itself may be difficult. In this case, the measurer must be very careful about the false interpretation.[66]

In this study, micro-CT was used. This non-destructive method uniquely enables to obtain three-dimensional information without additional sample preparation. Furthermore, various sectional views can be made without deformation of the specimen, and direct measurement is also possible.[65,67]

There is an inherent limitation of this study due to the micro-CT measurements. Reducing the pixel size enables to obtain a more accurate sectional view, however the minimum pixel size was limited. This study used 15.44 μm pixel size and many researchers used a 8-17 μm pixel size in the internal gap measurement with micro-CT.[34,65,67,68] This means it was possible to obtain proper resolution of images with an equivalent level of accuracy compared to previous studies.

V. CONCLUSIONS

Within the limitation of this study, the following conclusions were drawn. For SLA 3D printed resin prostheses, a difference in fit occurred based on the printing conditions. The desired printing conditions considering the marginal and internal fit were a 50 μm layer thickness with 45° and 60° build orientations. The same conclusion can be drawn with the SEM analysis because unintentional voids were created on the inner surface for 0° and 90° groups. When the SLA 3D printed prosthesis is manufactured with proper conditions, it is possible to obtain a comparable fit to the milled prosthesis. The fitness of both 3D printed and milled prostheses showed a clinically acceptable fit.

REFERENCES

1. Beuer F, Schweiger J, Edelhoff D. Digital dentistry: an overview of recent developments for CAD/CAM generated restorations. Br Dent J. 2008;204(9):505-11.
2. Duret F, Blouin JL, Duret B. CAD-CAM in dentistry. J Am Dent Assoc. 1988;117(6):715-20.
3. Orentlicher G, Abboud M. Guided surgery for implant therapy. Oral Maxillofac Surg Clin North Am. 2011;23(2):239-56.
4. Marchack CB. CAD/CAM-guided implant surgery and fabrication of an immediately loaded prosthesis for a partially edentulous patient. J Prosthet Dent. 2007;97(6):389-94.
5. Marchack CB. An immediately loaded CAD/CAM-guided definitive prosthesis: a clinical report. J Prosthet Dent. 2005;93(1):8-12.
6. Miyazaki T, Hotta Y, Kunii J, Kuriyama S, Tamaki Y. A review of dental CAD/CAM: Current status and future perspectives from 20 years of experience. Dent Mater J. 2009;28(1):44–56.
7. Pettenò D, Schierano G, Bassi F, Bresciano ME, Carossa S. Comparison of marginal fit of 3 different metal-ceramic systems: An in vitro study. Int J Prosthodont. 2000;13(5):405–8.
8. Atzeni E, Salmi A. Economics of additive manufacturing for end-usable metal parts. Int J Adv Manuf Technol. 2012;62(9-12):1147-55.
9. Van Noort R. The future of dental devices is digital. Dent Mater. 2012;28(1):3-12.

10. Stansbury JW, Idacavage MJ. 3D printing with polymers: Challenges among expanding options and opportunities. Dent Mater. 2016;32(1):54-64.
11. Nazir A, Abate KM, Kumar A, Jeng JY. A state-of-the-art review on types, design, optimization, and additive manufacturing of cellular structures. Int J Adv Manuf Technol. 2019;104(9-12):3489-510.
12. Jasveer S, Jianbin X. Comparison of different types of 3D printing technologies. Int J Sci Res. 2018;8(4):1-9.
13. Dawood A, Marti BM, Sauret-Jackson V, Darwood A. 3D printing in dentistry. Br Dent J. 2015;219(11):521-9.
14. Ji A, Zhang S, Bhagia S, Yoo CG, Ragauskas AJ. 3D printing of biomass-derived composites: application and characterization approaches. RSC Adv. 2020;10(37):21698-723.
15. Silva NR, Witek L, Coelho PG, Thompson VP, Rekow ED, Smay J. Additive CAD/CAM process for dental prostheses. J Prosthodont. 2011;20(2):93-6.
16. Xing H, Zou B, Li S, Fu X. Study on surface quality, precision and mechanical properties of 3D printed ZrO2 ceramic components by laser scanning stereolithography. Ceram Int. 2017;43(18):16340-7.
17. Klein HM, Schneider W, Alzen G, Voy ED, Günther RW. Pediatric craniofacial surgery: comparison of milling and stereolithography for 3D model manufacturing. Pediatr Radiol. 1992;22(6): 458-460.
18. Morris CL, Barber RF, Day R. Orofacial prosthesis design and fabrication using stereolithography. Aust Dent J. 2000;45(4):250-253.

19. Revilla-león M, Methani MM, Morton D, Zandinejad A. Internal and marginal discrepancies associated with stereolithography (SLA) additively manufactured zirconia crowns. J Prosthet Dent. 2020;124(6):730-7.
20. Kim SB, Kim NH, Kim JH, Moon HS. Evaluation of the fit of metal copings fabricated using stereolithography. J Prosthet Dent. 2018;120(5):693-8.
21. Khaledi AA, Farzin M, Akhlaghian M, Pardis S, Mir N. Evaluation of the marginal fit of metal copings fabricated by using 3 different CAD-CAM techniques: Milling, stereolithography, and 3D wax printer. J Prosthet Dent. 2020;124(1):81-6.
22. Moulding MB, Teplitsky PE. Intrapulpal Temperature During Direct Fabrication of Provisional Restorations. Int J Prosthodont. 1990;3(3):299-304.
23. Chiche GJ, Avila R. Fabrication of a preformed shell for a provisional fixed partial denture. Quintessence Dent Technol. 1986;10(9):579-81.
24. Burns DR, Beck DA, Nelson SK. A review of selected dental literature on contemporary provisional fixed prosthodontic treatment: report of the Committee on Research in Fixed Prosthodontics of the Academy of Fixed Prosthodontics. J Prosthet Dent. 2003;90(5):474-97.
25. Contrepois M, Soenen A, Bartala M, Laviole O. Marginal adaptation of ceramic crowns: a systematic review. J Prosthet Dent. 2013;110(6):447-54.
26. Mously HA, Finkelman M, Zandparsa R, Hirayama H. Marginal and internal adaptation of ceramic crown restorations fabricated with CAD-CAM technology and the heat-press technique. J Prosthet Dent. 2014;112(2):249-56.

27. Kocaagaoglu H, Kilinc HI, Albayrak H, Kara M. In vitro evaluation of marginal, axial, and occlusal discrepancies in metal ceramic restorations produced with new technologies. J Prosthet Dent. 2016;116(3):368-74.
28. Hunter AJ, Hunter AR. Gingival margins for crowns: a review and discussion. Part II: Discrepancies and configurations. J Prosthet Dent. 1990;64(6):636-42.
29. Tan K, Ibbetson R. The effect of cement volume on crown seating. Int J Prosthodont. 1996;9(5):445-51
30. Assif D, Rimer Y, Aviv I. The flow of zinc phosphate cement under a full-coverage restoration and its effect on marginal adaptation according to the location of cement application. Quintessence Int. 1987;18(11):765-74.
31. Gargallo-Albiol J, Barootchi S, Salomó-Coll O, Wang HL.Advantages and disadvantages of implant navigation surgery. A systematic review. Ann Anat. 2019;225:1-10.
32. Morton D, Jaffin R, Weber HP. Immediate restoration and loading of dental implants: clinical considerations and protocols. Int J Oral Maxillofac Implants. 2004;19:103-8.
33. Osman RB, Alharbi N, Wismeijer D. Build angle: does it influence the accuracy of 3D-printed dental restorations using digital light-processing technology? Int J Prosthodont. 2017;30(2):182-8.
34. Park GS, Kim SK, Heo SJ, Koak JY, Seo DG. Effects of Printing Parameters on the Fit of Implant-Supported 3D Printing Resin Prosthetics. Materials. 2019;12(16):2533.

35. Mai HN, Lee KB, Lee DH. Fit of interim crowns fabricated using photopolymer-jetting 3D printing. J Prosthet Dent. 2017;118(2):208–15.
36. Alharbi N, Alharbi S, Cuijpers VM, Osman RB, Wismeijer D. Three-dimensional evaluation of marginal and internal fit of 3D-printed interim restorations fabricated on different finish line designs. J. Prosthodont Res. 2018;62(2):218–26.
37. Kang SY, Park JH, Kim JH, Kim WC. Accuracy of provisional crowns made using stereolithography apparatus and subtractive technique. J Adv Prosthodont. 2018;10(5):354-60.
38. Park YW, You SW. Direction of improvement of reproducibility through shape distortion of fused deposition 3D printing. J Basic Design Art. 2018;19:195-204.
39. Tahayeri A, Morgan M, Fugolin AP, Bompolaki D, Athirasala A, Pfeifer CS, Ferracane JL, Bertassoni LE. 3D printed versus conventionally cured provisional crown and bridge dental materials. Dent Mater. 2018;34(2):192-200.
40. Alharbi N, Osman RB, Wismeijer D. Factors Influencing the Dimensional Accuracy of 3D-Printed Full-Coverage Dental Restorations Using Stereolithography Technology. Int J Prosthodont. 2016;29(5):503-10.
41. Brand RW, Isselhard DE. Anatomy of Orofacial Structures: A Comprehensive Approach. 7th ed. St. Louis:Mosby;2014.
42. Goodacre CJ, Campagni WV, Aquilino SA. Tooth preparations for complete crowns: an art form based on scientific principles. J Prosthet Dent. 2001;85(4):363-76.

43. Jang GJ, Kim SK, Heo SJ, Koak JY, Park JM. Investigation of optimal cement space in 3D printed 3-unit resin prosthesis: A Pilot Study. Journal of Korean Academy of Oral & Maxillofacial Implantology. 2020;24(2):62-75.
44. Unkovskiy A, Bui PHB, Schille C, Geis-Gerstorfer J, Huettig F, Spintzyk S. Objects build orientation, positioning, and curing influence dimensional accuracy and flexural properties of stereolithographically printed resin. Dent Mater. 2018;34(12):324-33.
45. Holmes JR, Bayne SC, Holland GA, Sulik WD. Considerations in measurement of marginal fit. J Prosthet Dent. 1989;62(4):405–8.
46. Hu J. Study on STL-based slicing process for 3D printing. In Proceedings of the 28th Annual International Solid Freeform Fabrication Symposium, Austin, TX, USA, 7–9 August 2017;p.885–95.
47. Wang WL, Cheah CM, Fuh JYH, Lu L. Influence of process parameters on stereolithography part shrinkage. Mater Des. 1996;17(4):205-13.
48. Huang Q, Zhang J, Sabbaghi A, Dasgupta T. Optimal offline compensation of shape shrinkage for three-dimensional printing processes. IIE trans. 2015;47(5):431-41.
49. Ishida Y, Miyasaka T. Dimensional accuracy of dental casting patterns created by 3D printers. Dent Mater J. 2016;35(2):250-6.
50. Zhai Y, Lados DA, Lagoy JL. Additive manufacturing: making imagination the major limitation. JOM. 2014;66(5):808-16.
51. Ligon SC, Liska R, Stampfl J, Gurr M, Mülhaupt R. Polymers for 3D printing and customized additive manufacturing. Chem Rev. 2017;117(15):10212-90.

52. Yang Q, Lu Z, Zhou J, Miao K, Li D. A novel method for improving surface finish of stereolithography apparatus. Int J Adv Manuf Technol. 2017;93(5):1537-44.
53. Mclean JW, Fraunhofer JA. The estimation of cement film thickness by an in vivo technique. Br Dent J. 1971;131(3):107-11.
54. Mitchell CA, Pintado MR, Douglas WH. Nondestructive, in vitro quantification of crown margins. J Prosthet Dent. 2001;85(6):575-84.
55. Baig MR, Tan KB, Nicholls JI. Evaluation of the marginal fit of a zirconia ceramic computer-aided machined (CAM) crown system. J Prosthet Dent. 2010;104(4):216-27.
56. Björn AL, Björn H, Grcovic B. Marginal fit of restorations and its relation to periodontal bone level. II. Crowns. Odontol Revy. 1970;21(3):337-46.
57. Boitelle P, Mawussi B, Tapie L, Fromentin O. A systematic review of CAD/CAM fit restoration evaluations. J Oral Rehabil. 2014;41(11):853–74.
58. Tuntiprawon M, Wilson PR. The effect of cement thickness on the fracture strength of all-ceramic crowns. Aust Dent J. 1995;40(1):17-21.
59. Juntavee N, Millstein PL. Effect of surface roughness and cement space on crown retention. J Prosthet Dent. 1992;68(3):482-6.
60. Sager B, Rosen DW. Use of parameter estimation for stereolithography surface finish improvement. Rapid Prototyp J. 2008;14(4):213-220.
61. Yildirim G, Uzun IH, Keles A. Evaluation of marginal and internal adaptation of hybrid and nanoceramic systems with microcomputed tomography: An in vitro study. J Prosthet Dent. 2017;118(2):200-7.

62. Kim JH, Jeong JH, Lee JH, Cho HW. Fit of lithium disilicate crowns fabricated from conventional and digital impressions assessed with micro-CT. J Prosthet Dent. 2016;116(4):551-7.
63. Shim JS, Kim JE, Jeong SH, Choi YJ, Ryu JJ. Printing accuracy, mechanical properties, surface characteristics, and microbial adhesion of 3D-printed resins with various printing orientations. J Prosthet Dent. 2020;124(4):468-75.
64. Hague R, Mansour S, Saleh N, Harris R. Materials analysis of stereolithography resins for use in rapid manufacturing. J Mater Sci. 2004;39(7):2457-64.
65. Pelekanos S, Koumanou M, Koutayas SO, Zinelis S, Eliades G. Micro-CT evaluation of the marginal fit of different In-Ceram alumina copings. Eur J Esthet Dent. 2009;4(3):278-92.
66. Laurent M, Scheer P, Dejou J, Laborde G. Clinical evaluation of the marginal fit of cast crowns: validation of the silicone replica method. J Oral Rehabil. 2008;35(2):116-22.
67. Borba M, Cesar PF, Griggs JA, Della Bona A. Adaptation of all-ceramic fixed partial dentures. Dent Mater. 2011;27(11):1119-26.
68. Seo D, Yi Y, Roh B. The effect of preparation designs on the marginal and internal gaps in Cerec3 partial ceramic crowns. J Dent. 2009;37(5):374–82.

SUPPLEMENTS

Table S1. Marginal fit of the 3D printed prostheses (mean ± SD μm)

Group		0°	30°	45°	60°	90°
AMD	50 μm	81.5 ± 15.1	79.0 ± 19.0	71.9 ± 8.3	105.0 ± 11.5	121.6 ± 12.5
	100 μm	99.1 ± 20.8	95.0 ± 12.5	78.4 ± 9.0	77.2 ± 8.5	114.2 ± 16.9
MG	50 μm	44.9 ± 13.1	48.4 ± 18.5	41.6 ± 7.2	61.5 ± 13.1	84.4 ± 12.3
	100 μm	66.1 ± 14.8	62.2 ± 12.4	52.7 ± 7.6	52.8 ± 8.4	82.1 ± 13.2

AMD: absolute marginal discrepancy, MG: marginal gap

Table S2. Axial gap of the 3D printed prostheses (mean ± SD μm)

Group		0°	30°	45°	60°	90°
CE	50 μm	122.1 ± 9.2	100.2 ± 8.0	85.2 ± 6.6	67.1 ± 8.4	84.0 ± 10.0
	100 μm	113.9 ± 6.3	105.2 ± 7.4	91.1 ± 10.4	83.7 ± 7.8	102.2 ± 10.4
AX	50 μm	115.0 ± 11.3	100.4 ± 8.4	89.8 ± 9.3	79.0 ± 8.2	85.0 ± 6.4
	100 μm	109.3 ± 8.6	112.8 ± 4.1	103.9 ± 12.4	92.9 ± 7.2	111.6 ± 7.8

CE: cervical area, AX: mid axial wall area

Table S3. Occlusal gap of the 3D printed prosthesis (mean ± SD μm)

Group		0°	30°	45°	60°	90°
LA	50 μm	68.8 ± 6.0	73.5 ± 12.3	77.3 ± 7.7	76.3 ± 6.8	66.7 ± 8.0
	100 μm	83.2 ± 7.2	102.3 ± 8.0	100.7 ± 11.7	83.9 ± 10.0	65.7 ± 6.5
OC	50 μm	112.6 ± 23.9	97.4 ± 25.5	126.9 ± 17.7	147.9 ± 15.2	175.7 ± 19.9
	100 μm	206.0 ± 16.7	170.8 ± 15.4	155.4 ± 29.7	134.9 ± 12.3	151.5 ± 21.8

LA: line-angle area, OC: occlusal area

Table S4. IGV of the 3D printed prostheses (mean ± SD mm^3)

Group	0°	30°	45°	60°	90°
50 μm	24.1 ± 1.4	22.5 ± 1.4	21.1 ± 1.3	20.2 ± 1.2	21.6 ± 1.3
100 μm	25.4 ± 1.4	25.5 ± 1.3	24.2 ± 1.8	21.8 ± 1.1	23.4 ± 1.3

IGV: internal gap volume

Table S5. Comparison of 3D printed and milled prostheses.

	3D printing 50 μm, 45°	3D printing 50 μm, 60°	Milling	*P*-value
IGV (mm^3)	21.1 ± 1.3	20.2 ± 1.2	19.6 ± 0.4	*$p = 0.014$
AMD (μm)	71.9 ± 8.3	105.0 ± 11.5	247.2 ± 7.4	***$p < 0.001$
MG (μm)	41.6 ± 7.2	61.5 ± 13.1	27.0 ± 6.7	***$p < 0.001$
CE (μm)	85.2 ± 6.6	67.1 ± 8.4	97.8 ± 3.8	***$p < 0.001$
AX (μm)	89.8 ± 9.3	79.0 ± 8.2	96.7 ± 2.6	**$p < 0.001$
LA (μm)	77.3 ± 7.7	76.3 ± 6.8	37.6 ± 6.5	***$p < 0.001$
OC (μm)	126.9 ± 17.7	147.9 ± 15.2	140.3 ± 12.3	@$p = 0.016$

IGV: internal gap volume, AMD: absolute marginal discrepancy, MG: marginal gap, CE: cervical area, AX: mid axial wall area, LA: line-angle area, OC: occlusal area. * indicates statistically significant difference between 50 μm, 45° printed and milled groups. ** indicates statistically significant difference between 50 μm, 60° printed and milled groups. *** indicates statistically significant difference between both printed and milled groups. @ indicates statistically significant difference between printed groups only.

-국문 초록-

Stereolithography 방식으로 제작된 3 본 레진 보철물의 다양한 3D 프린팅 적층 방향과 두께에 따른 적합도 분석

서울대학교 대학원 치의과학과 치과보철학 전공

(지도교수 김 성 균)

장 계 준

목 적 : 본 연구의 목적은 stereolithography (SLA) 방식의 3D 프린팅으로 제작한 3본 레진 보철물에서 적층 방향과 두께에 따른 적합도를 분석하는 것이다.

방 법 : 3본 고정성 레진 보철물을 장착할 수 있는 주모형을 5축 밀링 기계 (IDC MILL 5X; Amann girrbach AG, Koblach, Austria)로 절삭하여 제작하였다. 모델 스캐너 (T500; Medit, Seoul, Korea)로 주모형을 스캔한 후 상부 보철물을 CAD 소프트웨어 (Exocad Dental CAD; Exocad GmbH, Darmstadt, Germany)로 디자인하였다. 지대치의 장축과 제작 방향이 이루는 각도를 적층 방향으로 명명하였다. SLA 3D 프린터 (Zenith U; Dentis, Daegu, Korea)를 사용하여 다섯 가지 적층 방향 (0° , 30° , 45° , 60° , 90°)에 대해 두 가지 적층 두께 (50 μm, 100 μm)로 열 개 군, PMMA 레진 블록을 5축 밀링하여 (Arum DEG-5X100; Doowon, Seoul, Korea) 한 개 군의 보철물을 제작하였다. 총 11개 군에서 그룹 당 열 개씩 제작하였고 시편을 주모형에 적합 시킨 후 Micro-CT (Skyscan 1172; Bruker

micro-CT, Kontich, Belgium)를 이용하여 스캔하였다.

정량적 분석을 위해 변연과 내면 적합도는 imageJ 소프트웨어 (ImageJ 1.52 version; NIH, Bethesda, MD, USA)를 사용하여 측정하였다. 변연 적합도는 절대 변연 차이 (AMD), 변연 갭 (MG) 두 가지로 측정하였고 내면 적합도는 치경부 (CE), 축벽 중앙 (AX), 선각 (LA), 교합면 (OC) 부위에서 측정하였다. 축벽 중앙 (AX)은 보다 정확한 평가를 위해 내측/외측/협측/설측으로도 나누어 분석하였다. 내면 갭 부피 (IGV)는 CTAn 소프트웨어 (CTAn 1.17.7.2 version; Bruker micro-CT, Kontich, Belgium)로 측정하였다. 통계 분석으로 이원 분산 분석 및 T-검정을 시행하였고 신뢰수준은 95%로 하였다.

정성적 분석을 위해 각 시편의 관상면, 시상면, 수평면의 CT 단면을 조사하여 그룹 간 특징적인 차이를 비교하였다. 시편의 내면을 주사 전자 현미경 (Apreo S LoVac; Thermo Fisher Scientific, Brno, Czech)으로 촬영하여 미세구조적 특징을 비교 분석하였다.

결 과 : 절대 변연 차이 (AMD)는 가장 작은 값이 71.9 ± 8.3 μm (50 μm, 45°) 였고 가장 큰 값은 121.6 ± 12.5 μm (50 μm, 90°) 였다. 변연 갭 (MG)은 가장 작은 값이 41.6 ± 7.2 μm (50 μm, 45°) 였고 가장 큰 값은 84.4 ± 12.3 μm (50 μm, 90°) 였다. 모든 적층 두께에서 적층 방향 30° 와 45° 그룹이 보다 좋은 변연 적합도를 나타냈다. 가장 작은 치경부 (CE)갭은 67.1 ± 8.4 μm (50 μm, 60°) 였고 가장 큰 값은 122.1 ± 9.2 μm (50 μm, 0°) 였다. 가장 작은 축벽 중앙 (AX)갭은 79.0 ± 8.2 μm (50 μm, 60°) 였고 가장 큰 값은 115.0 ± 11.3 μm (50 μm, 0°) 였다. 모든 적층 두께에서 적층 방향 60° 그룹이 가장 작은 CE 및 AX 값을 나타냈다. 또한, 모든 프린팅 그룹에서 내측 축벽 중앙 갭이 외측 축벽 중앙 갭보다 항상 컸다 ($p < 0.001$). 시상면 축벽 중앙 갭은 적

층 방향이 0° 에서 60° 까지 증가함에 따라 작아지나 90° 로 증가할 때는 커졌다. 가장 작은 선각 (LA)갭은 65.7 ± 6.5 μm (100 μm, 90°) 였고 가장 큰 값은 102.3 ± 8.0 μm (100 μm, 30°) 였다. 가장 작은 교합면 (OC)갭은 97.4 ± 25.5 μm (50 μm, 30°) 였고 가장 큰 값은 206.0 ± 16.7 μm (100 μm, 0°) 였다. 가장 작은 내면 갭 부피 (IGV)는 20.2 ± 1.2 mm^3 (50 μm, 60°) 였고 가장 큰 부피는 25.5 ± 1.3 mm^3 (100 μm, 30°) 였다. 내면 갭 부피는 적층 두께에 상관없이 60° 의 적층 방향에서 가장 작은 값을 나타냈다. 적층 방향 0° 를 제외하면 적층 두께 50 μm 그룹에서 100 μm 그룹에 비해 작은 내면 갭 부피를 보였다.

바람직한 프린팅 조건에서 (50 μm, 45° 와 60°) AMD와 CE는 프린팅 그룹이 밀링 그룹에 비해 작은 값을 나타냈다. 그러나 MG와 LA는 프린팅 그룹이 밀링 그룹에 비해 큰 값을 나타냈다.

모든 프린팅 그룹의 CT 단면에서 계단 모양의 형태가 관찰되었고 이는 100 μm 적층 두께 그룹에서 50 μm 적층 두께 그룹에 비해 더 뚜렷하게 보였다. 또한, 밀링 그룹이 프린팅 그룹에 비해 평활한 표면을 보여주었다. 모든 프린팅 그룹의 수평면 CT 단면에서 내측 축벽 중앙 갭은 외측 축벽 중앙 갭 보다 크게 관찰되었다. 시상면 CT 단면에서 0° 적층 방향 그룹에서는 불균일한 교합면 내면이 관찰되었고 90° 적층 방향 그룹에서는 협측 내면에 큰 물결 모양의 고르지 않은 표면 형태가 관찰되었다. 주사 전자현미경 사진에서는 0° 적층 방향 그룹의 교합면 내면에서 빈 공간이 관찰되었고 90° 적층 방향 그룹의 협측 내면에서도 빈 공간이 관찰되었다. 또한, 90° 적층 방향 그룹의 교합면 내면에서 수직적인 선과 빈 공간이 관찰되었다. 빈 공간의 크기는 100 μm 적층 두께 그룹에서 50 μm 적층 두께 그룹에 비해 더 크게 나타났다.

결 론 : SLA 3D 프린팅 레진 보철물에서 적층 방향과 두께에 따른 적합도 차이가 발생하였다. 변연 적합도와 내면 적합도를 고려할 때, 바람직한 적층 방향은 45° 와 60° 였으며 적층 두께는 50 μm 였다. 주사 전자 현미경 분석에서도 0° 와 90° 적층 방향의 경우 내면의 의도치 않은 빈 공간이 형성되므로 동일한 결론이 도출된다. 적절한 적층 방향과 두께로 제작된 SLA 3D 프린팅 보철물은 밀링 보철물과 유사한 적합도를 보였다. 3D 프린팅 및 밀링 제작 보철물의 적합도는 모두 임상적으로 허용 가능한 범위 안에 있었다.

주요어 : Stereolithography; 3D 프린팅; Micro-CT; 적합도; 적층 방향; 적층 두께

학 번 : 2018-30853

감사의 글

박사과정을 무사히 마치고 이 논문을 시작하여 마무리하기까지 많은 도움을 주신 여러 스승님과 동료, 가족에게 감사의 말씀을 전합니다.

치과보철과 수련 및 대학원 생활에 있어 깊은 충고와 조언으로 진료와 연구에 귀중한 가르침을 주신 김성균 교수님께 깊은 감사를 드립니다. 병원 진료와 업무로 바쁘신 와중에도 본 논문을 위하여 많은 지도 편달을 해주셨습니다.

국소의치학이라는 학문의 깊이와 열정을 일깨워주시고, 이번 논문 심사에도 열과 성을 다해주신 허성주 교수님과 곽재영 교수님께도 깊은 감사를 드립니다.

바쁘신 와중에도 본 논문 심사를 위해서 꼼꼼히 살펴주신 치과생체재료학교실의 양형철 교수님과 경희대학교 치과대학의 김형섭 교수님께도 감사드립니다.

항상 따뜻한 격려와 조언을 해주신 치과보철학교실의 한중석 교수님, 임영준 교수님, 김명주 교수님, 권호범 교수님, 여인성 교수님, 윤형인 교수님, 이재현 교수님, 이유승 교수님과 치과보철학 교실원 여러분께 이자리를 빌어 감사의 말씀을 전합니다.

치과보철과 수련 기간동안 동고동락하며 서로에게 든든한 버팀목이 되어준 수련 동기 김웅규, 정민영, 홍영택, 홍정민 선생과 의국 선후배님들에게도 감사의 말씀을 전합니다.

오늘의 제가 있기까지 사랑과 정성으로 보살펴주시고 지원해주신 부모님께 깊은 감사를 드리며, 인생의 선배로서 항상 힘이 되는 형 장홍준과 저를 항상 응원해주는 동생 장정인에게도 고마움을 전합니다.

2021 년 1 월

장 계 준